

4-2021

**PARTIAL OXIDATION OF METHANE TO SYNTHESIS GAS OVER Ni/
 γ -Al₂O₃ CATALYSTS: THE EFFECT OF THE STRUCTURE AND THE
PRE-TREATMENT OF THE SUPPORT ON THE CATALYSTS'
PERFORMANCE**

Sheikh Tijan Jobe

Follow this and additional works at: https://scholarworks.uaeu.ac.ae/all_theses

 Part of the [Chemistry Commons](#)

Recommended Citation

Jobe, Sheikh Tijan, "PARTIAL OXIDATION OF METHANE TO SYNTHESIS GAS OVER Ni/ γ -Al₂O₃ CATALYSTS: THE EFFECT OF THE STRUCTURE AND THE PRE-TREATMENT OF THE SUPPORT ON THE CATALYSTS' PERFORMANCE" (2021). *Theses*. 845.
https://scholarworks.uaeu.ac.ae/all_theses/845

This Thesis is brought to you for free and open access by the Electronic Theses and Dissertations at Scholarworks@UAEU. It has been accepted for inclusion in Theses by an authorized administrator of Scholarworks@UAEU. For more information, please contact mariam_aljaberi@uaeu.ac.ae.

United Arab Emirates University

College of Science

Department of Chemistry

PARTIAL OXIDATION OF METHANE TO SYNTHESIS GAS OVER
Ni/ γ -Al₂O₃ CATALYSTS: THE EFFECT OF THE STRUCTURE AND
THE PRE-TREATMENT OF THE SUPPORT ON THE CATALYSTS'
PERFORMANCE

Sheikh Tijan Jobe

This thesis is submitted in partial fulfilment of the requirements for the degree of
Master of Science in Chemistry

Under the Supervision of Professor Abbas Ahmed Khaleel

April 2021

Declaration of Original Work

I, Sheikh Jobe, the undersigned, a graduate student at the United Arab Emirates University (UAEU), and the author of this thesis entitled “*Partial Oxidation of Methane to Synthesis Gas over Ni/ γ -Al₂O₃ Catalysts: The Effect of the Structure and the Pre-treatment of the Support on the Catalysts’ Performance*”, hereby, solemnly declare that this thesis is my own original research work that has been done and prepared by me under the supervision of Professor Abbas Ahmed Khaleel, in the College of Science at UAEU. This work has not previously been presented or published, or formed the basis for the award of any academic degree, diploma or a similar title at this or any other university. Any materials borrowed from other sources (whether published or unpublished) and relied upon or included in my thesis have been properly cited and acknowledged in accordance with appropriate academic conventions. I further declare that there is no potential conflict of interest with respect to the research, data collection, authorship, presentation and/or publication of this thesis.

Student’s Signature: S. Jobe

Date: 05-July-2021

Copyright © 2021 Sheikh Tijan Jobe
All Rights Reserved

Approval of the Master Thesis

This Master Thesis is approved by the following Examining Committee Members:

- 1) Advisor (Committee Chair): Abbas Khaleel

Title: Professor

Department of Chemistry

College of Science

Signature 

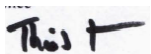
Date 05-July-2021

- 2) Member: Thies Thiemann

Title: Professor

Department of Chemistry

College of Science

Signature 

Date 05-July-2021

- 3) Member (External supervisor): Ahsan Ul Haq Qurashi

Title: Associate Professor

Department of Chemistry

Institution: Khalifa University, UAE

Signature 

Date 05-July-2021

This Master Thesis is accepted by:

Dean of the College of Science: Professor Maamar Benkraouda

Signature maamar Benkraouda

Date August 9, 2021

Dean of the College of Graduate Studies: Professor Ali Al-Marzouqi

Signature Ali Hassan

Date August 9, 2021

Copy ____ of ____

Abstract

Abundant natural gas is a potential source of more cost-effective energy and its effective utilization can significantly reduce the dependence on petroleum oil. Disadvantages of natural gas as a direct fuel include its low energy density by volume, and high cost of transportation, which resulted in its underutilization as an alternative energy source. Therefore, the conversion of methane to more easily-handled and value-added products is becoming a promising route for natural gas utilization. Compared to steam reforming of methane to syngas, which is the most commercially applied conversion process, partial oxidation is a more cost-effective promising route. While noble metals have been the most active catalysts, Ni-based catalysts are widely studied due to their lower costs. One of the drawbacks of such catalysts is their deactivation due, mainly, to carbon deposition and structural instability during reactions. Therefore, developing modified Ni-based catalysts to overcome these problems is an important objective for the development of commercially attractive catalysts. In the present work, the effect of the alumina support preparation and pre-treatment, and the effect of selected metal dopants on the Ni-support interaction, coke formation, and catalytic activity was studied.

Keywords: Partial Oxidation of Methane, Synthesis Gas, Natural Gas Conversion, Ni Catalysts.

Title and Abstract (in Arabic)

الأكسدة الجزئية للميثان وتحويله الى هيدروجين وأول أكسيد الكربون باستخدام

محفزات: Ni/ γ -Al₂O₃

تأثير داعم المحفز والمعالجة المسبقة للدعم على أداء المحفزات

الملخص

يعد الغاز الطبيعي الوفير مصدرًا محتملاً للطاقة الأكثر فعالية من حيث التكلفة ويمكن أن يقلل استخدامه الفعال بشكل كبير من الاعتماد على النفط البترولي. تشمل عيوب الغاز الطبيعي كوقود مباشر انخفاض كثافة الطاقة من حيث الحجم وارتفاع تكلفة النقل، مما أدى إلى عدم استخدامه كمصدر بديل للطاقة. لذلك، أصبح تحويل الميثان إلى منتجات يسهل مناولتها وذات قيمة مضافة أكثر طريقًا واعدًا لاستخدام الغاز الطبيعي. بالمقارنة مع إعادة تشكيل غاز الميثان بالبخار إلى غاز تخليقي، وهو أكثر عمليات التحويل تطبيقًا تجاريًا، فإن الأكسدة الجزئية هي طريق واعد أكثر فعالية من حيث التكلفة في حين أن المعادن النبيلة كانت أكثر المحفزات نشاطًا، إلا أن المحفزات القائمة على النيكل تتم دراستها على نطاق واسع نظرًا لتكلفتها المنخفضة. أحد عيوب هذه المحفزات هو تعطيلها بسبب ترسب الكربون وعدم الاستقرار الهيكلي أثناء التفاعلات. لذلك، فإن تطوير محفزات قائمة على النيكل للتغلب على هذه المشاكل هو هدف مهم لتطوير محفزات جذابة تجاريًا. في العمل الحالي، تمت دراسة تأثير تحضير دعامة الألومينا ومعالجتها المسبقة، وتأثير الإصابات المعدنية المختارة على تفاعل دعم النيكل، وتكوين فحم الكوك، والنشاط التحفيزي.

مفاهيم البحث الرئيسية: الأكسدة الجزئية للميثان، الغاز التخليقي، تحويل الغاز الطبيعي، محفزات النيكل.

Acknowledgements

My unreserved thanks and appreciation is extended to my supervisor Prof. Abbas Khaleel for the support and guidance he offered me throughout the preparation of this study.

Dedication

This thesis is dedicated to the memory of my beloved father. It is also dedicated to my Uncle, Sheikh Jobe for his continual support throughout my MSc program.

Table of Contents

Title	i
Declaration of Original Work	ii
Copyright	iii
Approval of the Master Thesis	iv
Abstract	vi
Title and Abstract (in Arabic)	vii
Acknowledgements	viii
Dedication	ix
Table of Contents	x
List of Tables	xii
List of Figures	xiii
List of Abbreviations	xv
Chapter 1: Introduction	1
Chapter 2: Literature Review	4
2.1 Methane Conversion Pathways	4
2.1.1 Selective Pathways	5
2.1.2 Non-Selectivity Pathways	7
2.2 Methane Reforming to Syngas	9
2.2.1 Steam Reformation	9
2.2.2 Dry Reformation of Methane	10
2.2.3 Combined Dry Reformation and Partial Oxidation	10
2.3 Catalytic Partial Oxidation of Methane	11
2.3.1 Background	11
2.3.2 Thermodynamics overview	12
2.3.3 Reaction Mechanism	13
2.3.4 Effects of Reaction Mechanism	14
2.4 Catalyst Preparation Method	15
2.4.1 Wet Impregnation	15
2.4.2 Co-Precipitation	16
2.4.3 Sol-Gel Process	17
2.5 Common Partial Oxidation of Methane Catalysts	18
2.5.1 Nickel-Based Catalysts	19
2.5.2 Bimetallic Catalysts	20
2.5.3 Noble Metal-Based Catalyst	20
2.5.4 Support Types	21

2.5.4.1 Alumina Supports	21
2.5.4.2 Zirconia Supports	22
2.5.4.3 Titanium Dioxide Supports	23
2.6 Catalysts Deactivations	23
2.6.1 Sintering	23
2.6.2 Carbon Deposition.....	24
Chapter 3: Experimental Methods	26
3.1 Introduction	26
3.2 Catalyst Preparation	26
3.3 Catalysts Characterization.....	28
3.3.1 X-ray Diffraction.....	28
3.3.2 H ₂ -Temperature Programmed Reduction.....	29
3.3.3 Thermogravimetric Analysis.....	30
3.3.4 Nitrogen-Sorption Analysis.....	31
3.3.5 CO Pulse Chemisorption	32
3.3.6 TEM and SEM Analysis	33
3.3.7 CO ₂ and NH ₃ -TDP	33
3.4 Catalytic Study	34
Chapter 4: Results and Discussion.....	37
4.1 Structural Characterization.....	37
4.2 Catalysts' Reducibility.....	42
4.3 Textural and Morphological Properties	46
4.4 CO Pulse Chemisorption.....	48
4.5 CO ₂ and NH ₃ TPD	51
4.6 In-situ DRIFTS of Chemisorbed CO	54
4.7 Catalytic Activity Tests.....	56
Chapter 5: Conclusion.....	65
References	67
List of Publications	75

List of Tables

Table 1: Proposed carbon-forming reactions	25
Table 2: Hydrogen consumption during H ₂ -temperature programmed reduction (H ₂ -TPR)	44
Table 3: Brunauer-Emmett-Teller (BET) surface area and pore characteristics of the reduced catalysts	45
Table 4: Metal dispersion, surface area, and crystallite size.....	48
Table 5: Total acidic sites and basic sites of catalyst and pure γ -Al ₂ O ₃	53
Table 6: Carbon deposit on spent catalysts	62

List of Figures

Figure 1: Methane conversion routes	5
Figure 2: Schematic diagram of HCN formation from methane	6
Figure 3: GTL and Fisher-Tropsch process route	8
Figure 4: Schematic diagram of non-selective methanol synthesis	8
Figure 5: Heat distribution in catalyst bed	13
Figure 6: Partial oxidation reaction mechanism	14
Figure 7: Scheme of the process for preparation of Ni/SiO ₂ and Ni/Al ₂ O ₃ catalysts	16
Figure 8: Synthesis of NiO-Al ₂ O ₃ mesoporous by modified sol-gel method	18
Figure 9: Comparison between activity, price, and selectivity of metal catalysts in partial oxidation of methane.....	18
Figure 10: Agglomeration of Ni particles at high temperature.....	24
Figure 11: Images of a typical sample after the different preparation steps.....	27
Figure 12: TGA instrument.....	31
Figure 13: Schematic diagram of the catalytic reaction setup	35
Figure 14: X-ray diffraction (XRD) patterns of Ni/ γ -Al ₂ O ₃ catalysts	38
Figure 15: X-ray diffraction (XRD) patterns of (A) Ni/ γ -AlOOH catalysts calcined after impregnation at temperatures (B) Ni/ γ -AlOOH-500 and Ni/ γ -AlOOH-950 compared with their counterparts based on γ -Al ₂ O ₃	39
Figure 16: X-ray diffraction (XRD) patterns of reduced Ni catalysts over (A) γ -Al ₂ O ₃ (B) γ -AlOOH and (C) over α -Al ₂ O ₃	41
Figure 17: H ₂ -TPR profiles of selected catalysts. A, (a) Ni/ γ -Al ₂ O ₃ -500 (b) Ni/ γ -AlOOH-500 (c) Ni/ γ -AlOOH-650 (d) Ni/ γ -Al ₂ O ₃ -650 (e) Ni/ α -Al ₂ O ₃ . B, Ni/ γ -Al ₂ O ₃ -950 and Ni/ γ -AlOOH-950.	42
Figure 18: TEM, A-C, and SEM, a-c images of reduced Ni/ γ -AlOOH-650, A,a, Ni/ γ -Al ₂ O ₃ -650, B,b, and Ni/ α -Al ₂ O ₃ , C,c.SEM, scanning electron microscopy; TEM, transmission electron microscopy.....	47
Figure 19: Schematic representation of the effect of the surface properties of the support precursor on the textural properties of the Ni particles.....	49
Figure 20: CO ₂ -TPD (A) and NH ₃ -TPD (B) profiles of the catalysts and pure γ - Al ₂ O ₃ . TPD, temperature-programmed desorption.....	52
Figure 21: (DRIFTS) spectra of adsorbed CO on selected reduced catalysts. (A) and a schematic representation of CO adsorption modes (B).....	54
Figure 22: Catalytic activity of Ni/ γ -Al ₂ O ₃ -derived catalysts at 700°C, 1 atm, and 7605 mL CH ₄ g ⁻¹ h ⁻¹ . Each measurement is an average of the results of three or four experiments with reproducibility around 98%.....	57
Figure 23: Catalytic activity of Ni/ γ -AlOOH-derived catalysts at 700°C, 1 atm, and 7605 mL CH ₄ g ⁻¹ h ⁻¹	59

Figure 24: Averages of CH ₄ conversion, products' selectivity, and H ₂ /CO ratio from 45-hour reactions over different catalysts at 700°C, 1 atm, and 7605 mL CH ₄ g ⁻¹ h ⁻¹	60
Figure 25: Carbon deposit on spent catalysts.....	62

List of Abbreviations

AlOOH	Boehmite
Al ₂ O ₃	Aluminum Oxide
CH ₄	Methane
Syngas	Synthesis Gas
SEM	Scanning Electron Microscopy
TDP	Temperature Programmed Desorption
TEM	Transmission Electron Microscopy
TGA	Thermogravimetric Analysis
TPR-H ₂	Temperature Programmed Reduction
XRD	X-ray Diffraction

Chapter 1: Introduction

The conversion of methane to syngas, a mixture of CO and H₂, by heterogeneous catalysis is a promising pathway of synthesizing chemicals such as methanol, organic solvents, acetic acid, and polymers. Most importantly, higher hydrocarbons can be derived from syngas using Fisher-Tropsch process, consisting of several chemical reactions to produce a wide variety of liquid hydrocarbons namely octane, olefins, alcohols, fuels including diesel, petrol, and kerosene. In addition, H₂ obtained from methane can be used as a clean energy source with no carbon emission. Given the vast natural gas sources worldwide, heavy research is being focused on methane because it is a viable solution to many of our contemporary environmental problems. Experts have predicted that methane shall surpass oil and petrol in terms of longevity, because of its plethoric reservoirs. It is relatively eco-friendly in comparison to the combustion of oil and petrol, making it a potential future energy resource.

Methane can be converted to higher hydrocarbons, with syngas as an intermediate, through different heterogeneously catalyzed chemical reactions. The reactant is methane in the gaseous state and the catalyst is in a solid form. Methane catalytic combustion, one of its conversion pathways can generally be classified into two types, partial oxidation and complete oxidation. This thesis is concerned with partial oxidation, implying incomplete combustion to produce 2 mols of H₂ and 1 mol of CO, from each mol of methane, accompanied with -36 KJ/mol in terms of energy. Catalytic partial oxidation is mildly exothermic and it occurs at high temperatures around 700°C. Conversely, complete oxidation is a highly exothermic process that releases large amounts of energy, CO₂ and H₂O.

In this study, Ni-based catalysts were employed to catalyze the reaction for several reasons. Ni-based catalysts are affordable and highly competent for methane conversion and highly competitive to the most active catalysts that are based on noble metals like Pt, Rh, Pd, and Ir. However, these metals are quite expensive. Therefore, Ni-based catalysts are widely employed in industrial catalysis. However, at elevated reaction temperatures, catalyst deactivation and undesirable side reactions occur due to coke formation that results in blocking of active sites and reactor plugging.

The main objective of our research is to develop Ni-based nano-particle catalysts with high stability and excellent performance for partial oxidation of methane. The catalysts were synthesized by wet impregnation of different alumina-based supports with Ni. The nature of the catalyst including its preparation, calcination temperature, textual properties, phase composition, and physicochemical properties, microstructure, metal dispersion, thermal stability, and electronic structure, all together govern the catalytical performance. The prepared catalysts were characterized by X-ray powder diffraction (XRD), temperature programmed reduction (TPR-H₂), thermogravimetric analysis (TGA), N₂ sorption analysis, scanning electron microscopy (SEM), transmission electron microscopy (TEM), temperature-programmed desorption TPD, and CO-chemisorption. XRD analysis characterizes phase composition and structures of the catalyst before reactions as well as phase modifications and structural changes during the reaction. The H₂-TPR was employed to assess the reducibility of the catalysts. TGA was used to measure the amount of carbon deposits on the catalysts during reactions. N₂ sorption was used to measure the surface area and to characterize the porosity. CO-pulse chemisorption was used to measure metal dispersion and metal surface area. SEM and TEM were used to characterize the catalysts' morphology. Finally, CO₂ and NH₃-TPD were used to

characterize acid-base properties of the catalysts' surface. Catalytic activity for partial oxidation of methane was studied using a fixed-bed flow reactor at 700°C under atmospheric pressure.

Chapter 2: Literature Review

Crude oil has been the major source of energy production for many centuries. It is usually refined to obtain petrol, diesel, and other petrochemical products. Due to high demand, crude oil reservoirs are expected to deplete. Therefore, oil and petrol prices are sharply increasing. Apart from its limited reserves and high cost, crude oil produces tons of waste products and releases harmful toxins into the environment. Fortunately, this practice is about to change, as over the last three decades natural gas usage has been gradually increasing. Natural gas is the cleanest of all hydrocarbons. This makes it a promising source for energy generation. In addition, it can serve as a fuel for vehicles as well as a chemical feedstock for chemical synthesis. Furthermore, replacing oil with natural gas would eliminate the need for oil importation, bringing economic advantages. There are abundant natural gas reservoirs present in many countries, especially in the USA, Norway, Russia, China, and all GCC countries. These huge reservoirs can last for more than a hundred years. We can expect natural gas as the new driving force for power generation, for the petrochemical, and fuel production industry [1].

2.1 Methane Conversion Pathways

One of the main challenges associated with methane conversion is its stable tetrahedral structure. The strong carbon-hydrogen bonds require large amounts of energy to dissociate. Methane conversion to value-added products can still be accomplished through a direct and an indirect pathway [2]. The former is a direct conversion of methane to the desired product and the latter is a multistep procedure that relies on the conversion of methane into an intermediate, followed by conversion

of the intermediate to the desired product. Figure 1 displays a summary of the possible products that can be derived from methane.

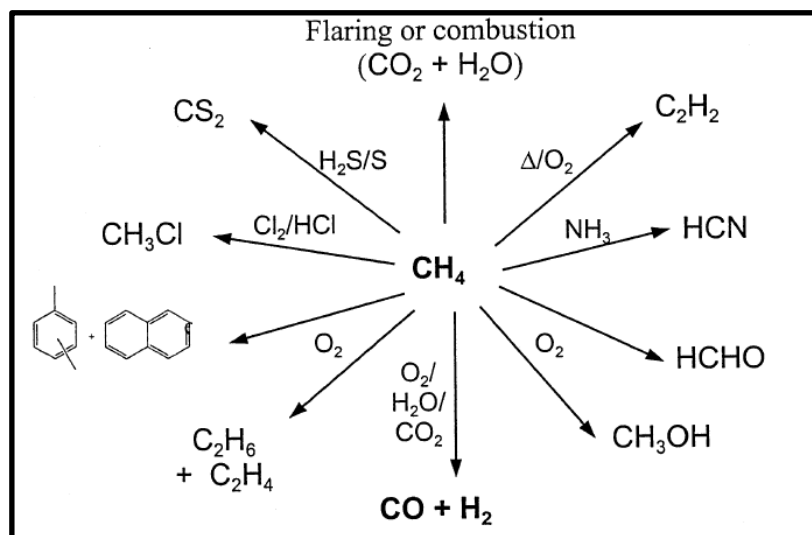


Figure 1: Methane conversion routes [3]

2.1.1 Selective Pathways

Selective reaction pathways involve a series of successive steps leading to the desired product. Selective reactions offer the ability to control the choice and distribution of the products by altering the reaction condition. One of the early examples of selective methane conversion was the Andrussov process, developed in the year 1927, to selectively synthesize HCN from methane and ammonia in an oxygen-rich medium catalyzed by Pt-based catalysts. The reaction is highly endothermic and it occurs between 1000-1200°C at 2 atm [4]. The overall reaction is presented in Figure 2. As the reaction progresses, after the first 40-80 hours, around 60% of methane is converted to HCN.

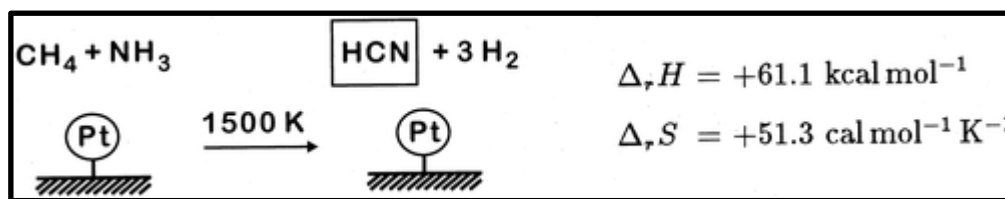
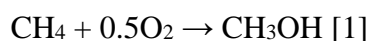


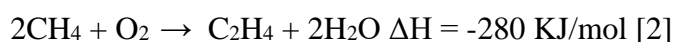
Figure 2: Schematic diagram of HCN formation from methane [5]

Moreover, HCN can be converted to other chemicals such as acrylonitrile, methyl methacrylate and adiponitrile which are used as precursors to synthesize polymers, textile fibers and other materials.

Another attempt of direct methane conversion was known as controlled oxidation. It was developed in the 1980s to convert methane to methanol [6]. The high demand for methanol at that time and the large reserves of natural gas prompted researchers to find direct methane conversion pathways. Side reactions do occur during the process but overall, the reaction produces CH_3OH , HCHO , CO_2 and CO in yields of 85, 10, 3 and 2 %, respectively. Methane is partially oxidized to methanol as shown in Equation 1.



Oxidative coupling was another chemical reaction developed in the 1980s to convert methane directly to C_2 hydrocarbons to yield ethylene, an essential starting material in the petrochemical industry [7]. Peculiarly, ethylene is much more reactive than its precursor. The product formed during the reaction reacts further, hence the overall yield is low. The reaction is represented in Equation 2 and it was conducted between 750-950°C.



Currently, there is no well-established process that allows direct conversion of methane. Many processes have been attempted but none of them was capable of reaching high yields or has proven to be cost-effective.

2.1.2 Non-Selectivity Pathways

Gas to liquid (GTL) is a process of producing long-chain hydrocarbons from natural gas [8]. GTL is a well-established technology and many GTL plants have been built around the globe [9]. The GTL process consists of three steps. The first step is syngas generation, next is the Fischer-Tropsch synthesis, followed by product workup which involves purification and refining to convert syngas to a wide spectrum of commodities such as naphtha, petrol, diesel, detergents, lubricants, propylene, alpha olefins and dimethyl ether [10]. Of the three steps, the production of syngas is the most expensive due to, mainly, high energy demand. Therefore, methods with a lower cost of syngas production are being investigated [11].

One of the steps of GTL technology is the Fischer-Tropsch process, a chemical process developed by Franz Fischer and Hans Tropsch in Germany, in 1927-1945 [12]. It is a catalytic polymerization and hydrogenation process of carbon catalyzed by Co or Fe at temperatures in the range of 150-300°C and pressures of 1 to 10 atm. Operation at high temperature increases the rate of the reaction and the conversion rate, but it also leads to methane formation. To circumvent this problem, it is suggested to carry out the reaction at relatively lower temperatures [13]. Relatively high pressure is advised, because it leads to high conversion rates and longer hydrocarbon chains. Before the process is initiated, syngas must be at the proper stoichiometric ratio of hydrogen and carbon monoxide of 2.0 and the composition has to be purified to

eliminate unwanted species, that might disturb the downstream process or even poison the catalysts. A typical scheme of GTL and Fischer-Tropsch is presented in Figure 3.

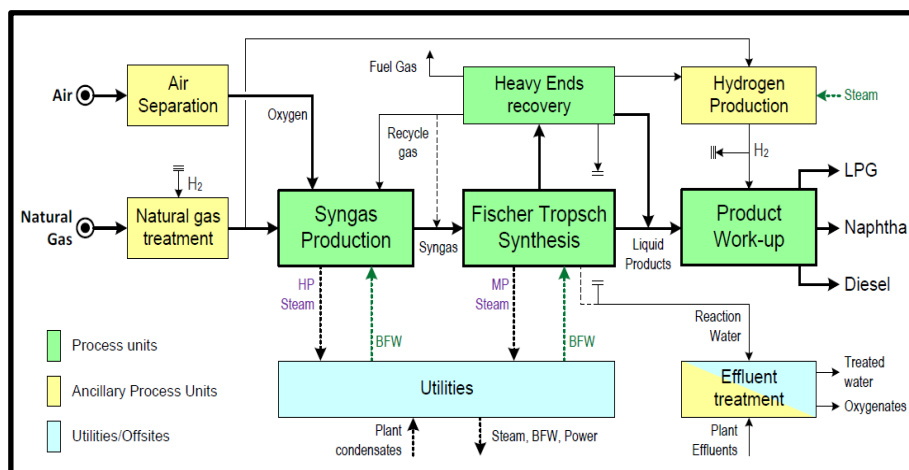


Figure 3: GTL and Fisher-Tropsch process route [1]

One of the downstream processes involves methanol synthesis in a multi-step pathway using Cu-ZnO-based catalysts [14]. The first step is reforming of methane to syngas, followed by conversion of the syngas intermediate into methanol. In the final step, the crude methanol is extracted and purified. Presently, methanol is a valuable commodity in the chemical industry used to synthesize adhesives, paints, silicones, formaldehyde, dimethyl ether, and other important chemicals. A schematic representation of the process is shown in Figure 4.

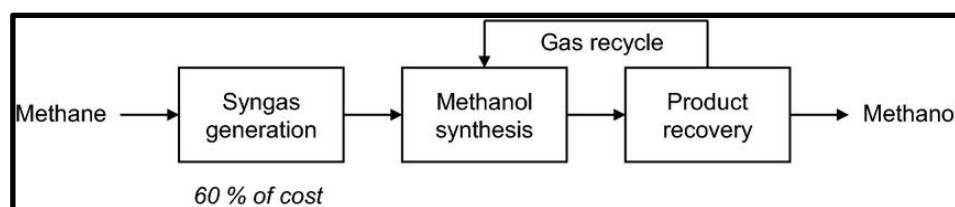


Figure 4: Schematic diagram of non-selective methanol synthesis [15]

2.2 Methane Reforming to Syngas

Methane is a greenhouse gas associated with environmental problems. One of the ways to put methane to good use is to convert it into syngas. This section provides a brief overview of the three most well-known processes for methane reformation to syngas: steam reformation, dry reformation and the combined dry reformation-partial oxidation method.

2.2.1 Steam Reformation

Steam reformation is the earliest and most widely used industrial technology for syngas production. In fact, it is the only commercial syngas production method and it occurs at high temperatures, which makes methane to syngas conversion thermodynamically favored. Also, the steam reformation system does not require an input of oxygen, therefore it eliminates the need of a separation unit [3].

The problem associated with steam reformation is that it is an endothermic process. For this reason, more energy friendly methods are being explored such as the partial oxidation method. Secondly, the H₂/CO ratio has to be adjusted to 2 for downstream processes by using additional reactions to attain the desired ratio.



The water gas shift reaction shown in Equation 4 is mildly exothermic. The product composition depends on the reactor temperature, pressure and composition. Overall, the reaction yields a mixture of CO, CO₂, H₂, unreacted CH₄ and steam [2]. Common catalysts used for steam reformation include Ni, Ir, Pd, Rh, Co and Pt. Metal

oxides with high oxygen storage capacity namely, CeO₂ and ZrO₂ are used to improve the carbon-resistant properties of catalysts.

2.2.2 Dry Reformation of Methane

The dry reformation process is an interesting technology because it converts both greenhouse gases; methane and CO₂ to syngas [3]. In other words, methane reacts with carbon dioxide to give carbon monoxide and hydrogen gas, as shown in Equation 5.



The dry reformation process is an endothermic reaction and requires high temperatures of 600 to 900°C. Also, the ratio of CO and H₂ is 1:1, therefore it has to be adjusted for further downstream processes [2]. Moreover, a highly stable catalyst with appreciable catalytic activity is difficult to find for this process due to excessive coking which leads to reaction deactivation. Ni/Al₂O₃ synthesized by sol-gel method, is commonly used for the dry reformation reaction owing to its low cost, but it suffers severely from carbon deposition. Noble metals such as ruthenium (Ru) and rhodium (Rh) are frequently encountered in this process as well, due to their coke-resistant properties.

2.2.3 Combined Dry Reformation and Partial Oxidation

Dry reformation is often combined with partial oxidation catalyzed by Ni/-γ-Al₂O₃ to achieve enhanced syngas production. Combining the endothermic dry reformation with the exothermic partial oxidation significantly lowers the energy required for the overall process [1-3]. Most importantly, the addition of oxygen into the dry reformation feed system has proven to decrease the coke formation reactions

via re-oxidation to prevent blockage of the active sites of the catalysts [1]. Combining partial oxidation with dry reformation aids in the elimination of hot spots and temperature gradients. Different catalyst supports such as Al_2O_3 , MgO , SiO_2 have all been tested. The right catalyst support and appropriate catalyst preparation method can yield excellent physiochemical properties with good stability and high catalytical activity [11].

2.3 Catalytic Partial Oxidation of Methane

2.3.1 Background

The early experiments on catalytic partial oxidation were conducted by Liander, Padovani, Feranchetti and Prette. They discovered that synthesis gas with a H_2/CO ratio of 2 could be produced between 1000-1200K at 1 atm, using Ni catalysts [3, 16]. Years later, researchers confirmed the observations of the early experiments and also discovered that Ni favored carbon formation. After that, Lunsford and co-workers investigated Ni catalyst supported on alumina at 720-1173K. They reported that the optimum temperature was 973K for partial oxidation. At that time, the conventional route for syngas production was the endothermic steam reforming process, but the process was flawed by its low efficiency in terms of product yield, requirement of high temperature over 900°C , and prohibitively high pressures of 20 to 40 bars. These reaction conditions were costly and difficult to maintain. The newly discovered catalytic partial oxidation route was regarded as an alternative to the steam reforming process. Further studies were conducted by Lunsford and co-workers using Ni catalysts, they observed excellent results with; CO selectivity near to 97% and almost complete methane conversion going past 973K temperature. Many researchers

confirmed the reproducibility of their work and they all arrived at the same conclusions [3].

2.3.2 Thermodynamics overview

The early experiments on catalytic partial oxidation of methane left some questions to be answered namely, the reaction mechanism, the cause of hotspots in the catalyst bed and coking during the reaction. To answer these questions, the thermodynamics of the partial oxidation has to be explained, in order to comprehend the chemical reactions and the energy changes involved. Deactivation caused by carbon deposition was not investigated in detail because at that time, steam reforming was well established, and therefore, studying partial oxidation was suspended for decades. In 1980, Green and co-workers revived the study of partial oxidation. Their catalyst of choice was $\text{Ln}_2\text{Ru}_2\text{O}_7$, which showed excellent catalytic activity no carbon deposition that could be spotted by the naked eye on the spent samples. Confirmation of the absence of carbon was done using high-resolution electron microscopy. Their results led to the investigation of the reaction mechanism and the effects of reaction conditions on partial oxidation. The findings from the thermodynamic study reaped a wealth of information. The calculations suggested that using a high temperature, in the range of 973-1200K was recommended to produce high methane conversion and selectivity to CO and H_2 . In contrast, increasing the pressure in the reactor was unfavorable for CH_4 conversion as well as, CO and H_2 selectivity. At 1073K, under 1 bar pressure, the theoretical CH_4 conversion was expected to be approximately 90% and selectivity to CO and H_2 at 97%. At 1073K, under 8 bar pressure, the theoretical CH_4 conversion was expected to be around 70% and selectivity to CO and H_2 around 85%.

The thermodynamic analysis identified the presence of hotspots within the catalyst bed in the reactor, where elevated temperatures were measured at different spots. Referring to the early study conducted by Prettre et al. in 1945, the challenge was to explain the large variation or the different heat gradients across the catalysts bed. The authors extrapolated that partial oxidation is a combination of exothermic and endothermic reactions. The presence of hot spots indicated that complete oxidation of methane took place to release a colossal amount of heat [1, 3]. At the extremes of the catalyst bed, the temperature was found to be significantly lower due to the endothermic steam reforming reaction which absorbed heat as shown in Figure 5.

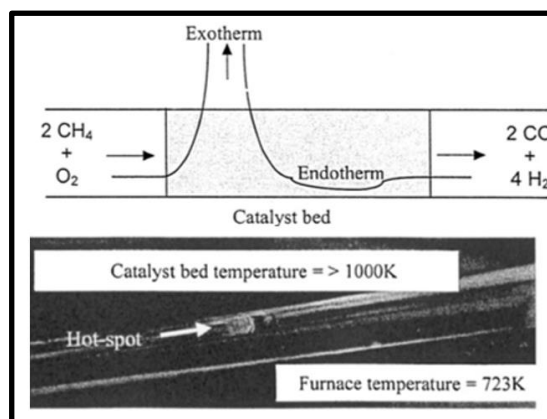


Figure 5: Heat distribution in catalyst bed [3]

2.3.3 Reaction Mechanism

As discussed above, the overall temperature of the catalyst bed was not uniform indicating a two-step reaction. It was proposed that, methane was first completely oxidized to CO_2 and H_2O in an exothermic reaction, followed by reforming of methane to syngas in the absence of oxygen under the activity of a metal oxide that behaved as an oxygen storage as shown in Equation 6-8 [17, 18].





A mechanism consisting of a combustion-reforming reaction was firmly accepted by many authors as presented in Figure 6.

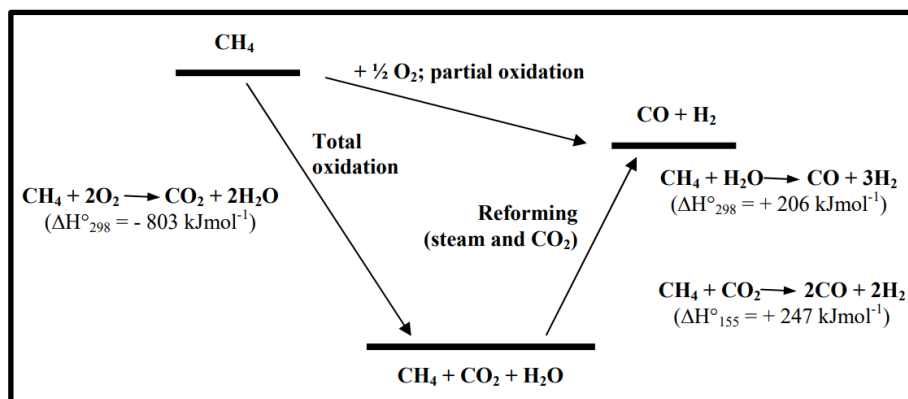


Figure 6: Partial oxidation reaction mechanism [17]

2.3.4 Effects of Reaction Mechanism

The temperature has a significant impact on the reaction mechanism, CH₄ conversion, and CO and H₂ selectivity. The optimum temperature of the reaction and minimum temperature needed to overcome the activation energy depends on the type of catalyst and the reaction conditions. In general, as the temperature increases, partial oxidation is more thermodynamically favored because the CH₄ conversion and the CO and H₂ selectivity increase [19]. However, the CH₄ conversion and the CO and H₂ selectivity are all inversely proportional to the pressure, which is usually kept at 1 atm. Elevating the reactor pressure causes a decrease in the conversion of CH₄ and selectivity to CO and H₂. It is suggested to even evacuate the product species to improve the performance. Most importantly, there must be an appropriate balance of

CH₄ and O₂. A CH₄/O₂ ratio of 2 is recommended for partial oxidation to produce syngas.

2.4 Catalyst Preparation Method

It is always necessary to use the optimum preparation parameters to ensure the maximum efficiency of the catalysts. The target is to achieve desired textural properties that can lead to high catalytic activity, selectivity, and thermal stability. This section discusses three common preparation methods, namely wet impregnation, co-precipitation and sol-gel process.

2.4.1 Wet Impregnation

This method involves a three-step procedure to prepare supported metal catalysts. Firstly, an appropriate amount of the active metal precursor is dissolved in an appropriate solvent, usually water. Metallic precursors are usually inorganic salts of the metal such as metal carbonates and nitrates [20]. The solution is well mixed to improve homogeneity especially when bi-metallic catalysts are prepared. The solution is used to impregnate the support by adding the solution drop-wise to load the support with the metal component followed by thorough mixing to form a paste. After that, drying the mixture is followed by calcination conducted at the desired temperatures to eliminate any volatile components in the mixture, to obtain the metal oxide, and to stabilize and strengthen the interactions of the active species with the support [21]. Wet impregnation is the most common catalyst preparation method employed for the synthesis of supported Ni-based catalysts on alumina or other types of supports due to its simplicity. In addition, the catalyst's components, alumina and the metal nitrates, are of relatively low cost and are easily available. Furthermore, the metal nitrates are

highly soluble and nitrates decompose easily during calcination. Figure 7 illustrates the procedure of Ni/Al₂O₃ and Ni/SiO₂ preparation, as examples. The main drawback of this method is that it can result in uneven distribution of the active species, making it unsuitable for the preparation of catalysts with high metal loading. High loading leads to poor dispersion, which is the ratio of the number of surface metallic atoms to the total number of atoms [22].

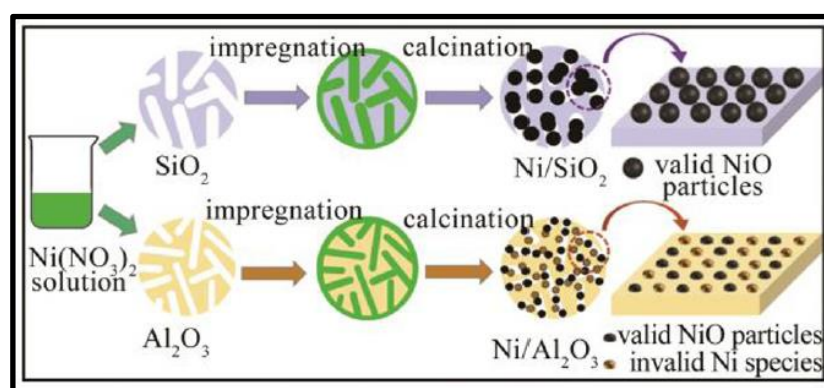


Figure 7: Scheme of the process for preparation of Ni/SiO₂ and Ni/Al₂O₃ catalysts [21]

2.4.2 Co-Precipitation

The co-precipitation method is among the oldest methods, but it is still widely used to prepare supported catalysts [20]. The process is centered on mixing the aqueous phase of the metallic salt with a support precursor solution to form an insoluble metal species such as hydroxide or oxide. The first step is to dissolve the metal precursors usually in the form of metal nitrate in water or any other suitable solvent to form a homogeneously distributed mixture of the active components. The precipitation process is induced by alterations of some of the mixture parameters such as temperature, pH or salt concentration to initiate particles' growth and agglomeration. The filtration and drying of the precipitate to obtain the dry product,

which is followed by calcination to convert the product, which is usually a metal hydroxide, to a metal oxide. A reduction reaction is conducted to achieve the metallic elements, if so desired [23]. This method can be used to prepare different catalytic materials such as Ni/Al₂O₃ for steam reforming and partial oxidation. Cu/ZnO/Al₂O₃ for methanol synthesis and Fe–Cu–K for Fisher-Tropsch synthesis [24, 25]. The disadvantage of this method is that the precipitate formation is not an easily controlled process. Hence, uncontrollable particle morphology, agglomeration and uneven distribution of metal ions are bound to occur [26].

2.4.3 Sol-Gel Process

Sol-gel has become the standard preparation technique for many materials, even though it was initially used for synthesizing SiO₂. Nowadays, it is used to prepare biomaterials, glass, ceramic, polymers and fibers [27]. Its applications even extend to the semiconductor industry to synthesize semiconductors like ZnO₂, WO₃ and SnO₂. It has wide applications in heterogeneous catalysis for preparing metal oxides with a high degree of dispersion. For example, alumina, TiO₂, ZnO₂, perovskites and mesoporous materials can be prepared using the sol-gel method. The sol-gel chemistry involves a solution and gel phases. It involves different steps that take place in the following order: hydrolysis, polycondensation, gelation, aging and drying as shown in Figure 8. The starting solution turns first into a sol mixture, which is basically a colloidal suspension containing the solid particles. The sol then turns into a gel phase, which is composed of interconnected solid colloidal particles containing the solvent within cavities. The choice of the precursor is important to form gels. Metal alkoxides have been widely employed in sol-gel preparation of oxides, such as alumina and silica, where upon hydrolysis, a homogeneous 3-dimensional gel network can be

obtained. Highly porous aerogels can be obtained if the solvent is removed from the gel by supercritical drying at the critical temperature and pressure of the solvent. The sol-gel method is well established in the field of heterogeneous catalysis. It allows synthesis of catalysts as intended because it offers the possibility of modifying the preparation conditions such as solution pH, type of solvent, reaction concentrations, temperature and aging time to control the active sites, porosity structure, surface area, particle shape, dispersion, texture and homogeneity as desired [20].

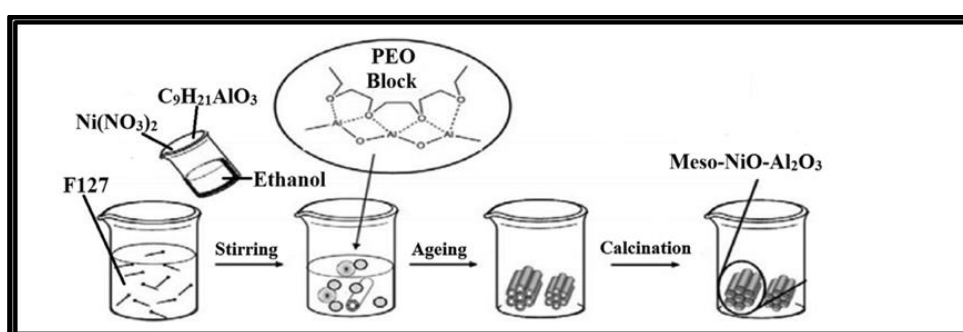


Figure 8: Synthesis of NiO-Al₂O₃ mesoporous by modified sol-gel method [27]

2.5 Common Partial Oxidation of Methane Catalysts

The catalysts that have been widely investigated for partial oxidation of methane can be divided into two categories as shown in Figure 9. Catalysts can be based on the transition metals including Ni, Fe, Co and the noble metals namely, Ir, Pt, Pd, Pt and Rh.

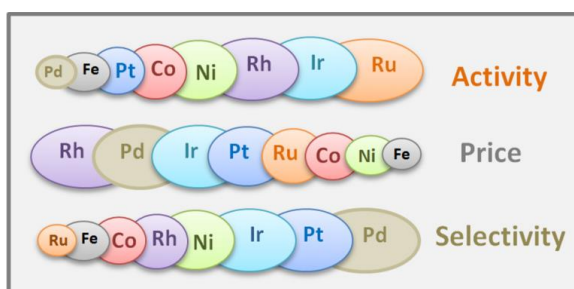


Figure 9: Comparison between activity, price, and selectivity of metal catalysts in partial oxidation of methane [28]

2.5.1 Nickel-Based Catalysts

Nickel has been the most widely studied active metal for partial oxidation of methane. It has been the most favored catalyst due to the good balance between its performance and the low cost of Ni. These advantages allowed Ni-based catalysts to be competitive candidates for replacing noble metals [29]. Ni/ γ -Al₂O₃ catalysts, where Ni is supported on the surface of γ -alumina, are widely used in methane conversion research, including the partial oxidation of methane. They usually show good thermal stability, high surface area and well dispersed metallic Ni particles over the alumina support. However, there are some shortcomings associated with Ni-catalysts supported on γ -alumina during reactions including sintering, coke formation, phase transformation of the support and formation of large aggregates of the active species [30]. Therefore, Ni catalysts supported on α -Al₂O₃ are used for industrial applications due to their structural stability under harsh reaction conditions [31]. However, α -Al₂O₃ is a highly crystalline solid and possesses very low surface area and negligible inter-particle porosity [32].

Ni supported on MgO prepared by sol-gel method has also been studied [33]. MgO is known for its high thermal stability and readily forms solid solutions with NiO because of their compatible structural characteristics, making it possible to achieve dispersed Ni crystallites after reduction. In other words, the Ni settles in the MgO lattice and is homogeneously spread in the catalyst. One of the major advantages of MgO as a support is its ability to suppress carbon deposition which has been referred to the basic properties of MgO [34].

2.5.2 Bimetallic Catalysts

Incorporating metals such as Ce, Fe, V, Cr and Mn to form Metal-Ni alloys can improve overall catalytical performance [35]. Ni-Ce based catalysts demonstrate incredible thermal stability, good redox properties and are renowned for their oxyphilic nature which equips them with anti-carbon properties [22]. The oxygen sites situated at the metal-support interface are easily reducible during the reaction, the oxygen sites near the active metal expel the deposited carbon from the catalyst surface to improve the coke resistant properties of the catalysts.

Ni-based catalysts derived from perovskite-type oxides (ABO_3) like $LaNiO_3$ are known for producing small metallic particles after reduction with high dispersion on the surface of the oxide support, thereby suppressing sintering and formation of coke [36]. $LaNiO_3$ shows outstanding catalytic performance in methane partial oxidation reactions. After reduction, the Ni species can be trapped in the La_2O_3 matrix forming strong interactions with the supports.

Ferrerira et al., studied methane partial oxidation over copper-actinide based catalysts, and it was observed that copper had a lower performance compared to Ni-based catalysts. The lower activity was referred to the fact that dissociation of methane on copper is endothermic while it is exothermic on nickel [37, 38].

2.5.3 Noble Metal-Based Catalyst

The most active catalysts for partial oxidation of methane are based on costly noble metals like Rh, Pt and Pd supported on alumina, magnesia or zirconia [35]. It is agreed that noble metals demonstrate outstanding high activity and resistance to coke formation. There is a significant number of studies in the literature on Pt-based

catalysts namely, Pt/Al₂O₃, Pt/ZrO₂ and Pt/Ce-ZrO₂ [38]. It is reported that Pt/Ce-ZrO₂ demonstrated phenomenal performance owing to the role of Ce in enhancing its reducibility and oxygen vacancies near the metal particles contact with the oxide, which helps in getting rid of carbon and keeping the surface clean. Pt/Ce-ZrO₂ showed higher activity, stability and selectivity compared to the Pt/Al₂O₃ and Pt/ZrO₂ [39].

2.5.4 Support Types

The most widely studied supports for metal catalysts are Al₂O₃, TiO₂ and ZrO₂. The purpose of the support is to serve as a host for the active component, increasing the dispersion, specific surface area and stability of the catalyst [40]. The support is evaluated based on the specific surface area, porosity, particle size and shape, and mechanical and thermal stability.

2.5.4.1 Alumina Supports

Aluminum oxide, which is polymorphic, is widely used as a catalyst support due to its excellent properties including high surface area, adjustable pore structure, outstanding adsorption ability and high stability in most oxidation reactions [41]. The γ -Al₂O₃ phase can be prepared by calcination of commercial Boehmite (AlOOH) at 500°C. Further calcination results in conversion to other phases, and heat-treatment beyond 1100°C will result in its transformation to the α -Al₂O₃ phase, which is the most stable of all alumina phases with excellent thermal stability and anti-carbon properties [42]. However, it shows a lower performance compared to the γ -Al₂O₃ due to its low surface area and high crystallinity.

2.5.4.2 Zirconia Supports

Zirconia supports are well known for catalytical applications due to their acid and basic character and redox properties [43]. Zirconia has excellent physical-chemical properties and exhibits phenomenal catalytical properties that are highly dependent on its crystal phase. ZrO_2 has three polymorphs the monoclinic phase, the tetragonal phase, and the cubic phase. It has been reported that the tetragonal phase which occurs at temperatures between $1170^\circ C$ to $2370^\circ C$ is the most active phase for catalytic applications due to its higher concentration of acidic sites and oxygen vacancies [44]. Ni/ ZrO_2 - Al_2O_3 catalysts have been reported; whereby, ZrO_2 is often used to make core-shell structured catalysts which are known for their anti-sintering and anti-coke properties owing to their confinement effect ability. For example, zirconia-modified nanoparticles are used as core particles and microporous silica are used as shells. The ZrO_2 confines the Ni active sites in the silica shell to enhance stability. Ni- ZrO_2 @ SiO_2 catalysts prepared by one-pot method demonstrated excellent stability for 240 hours dry reforming of methane [45]. No coke deposition or Ni species aggregation was observed. Combining the Al_2O_3 and ZrO_2 support in a mixed oxide was found to lead to superior catalytic properties. Ni/ ZrO_2 - Al_2O_3 support catalysts showed high surface area, basicity, and high thermal stability [46]. Furthermore, the effects of CeO_2 - ZrO_2 and γ - Al_2O_3 mixing for partial oxidation of methane has been studied by preparing Ni/ CeO_2 - ZrO_2 / γ - Al_2O_3 . The small size of Al^{3+} allows it to settle into the CeO_2 - ZrO_2 lattice to form defects and oxygen vacancies when CeO_2 - ZrO_2 and γ - Al_2O_3 are mixed. Hence, oxygen mobility from the bulk to the surface enhances its anti-coke properties by preventing sintering of Ni and oxidizing coke to CO_2 owing to the high oxidizing capability [47].

2.5.4.3 Titanium Dioxide Supports

TiO₂ also known as titania, is a reducible oxide with three polymorphs namely anatase, brookite and rutile [48]. Although, TiO₂ is not used as commonly as Al₂O₃, there are a few studies in the literature where TiO₂ was used as a support for partial oxidation reactions owing to its high surface area, chemical stability, acid-base properties, redox properties and high abundance [49]. Ni/TiO₂ and Rh/TiO₂ have been used for partial oxidation reactions and CO reforming. TiO₂ supports show strong metal-support interaction which suppresses coking. However, the anatase phase reacts with NiO to form NiTiO₃ at temperatures between 800-1100°C. Also, transformation of anatase to rutile occurs between 750-1200°C [50, 51].

2.6 Catalysts Deactivations

The major challenge in most heterogeneous catalysis is to overcome catalyst deactivation, which occurs due to different reasons. The major causes of deactivation are particles sintering and coke deposits, which also lead to reactor plugging.

2.6.1 Sintering

Sintering is the growth of supported metal nanoparticles resulting in a decrease in metallic specific surface area, pore size and loss of catalytic activity, especially for high temperature catalytic processes. The metal particles fuse together below their melting point. Two mechanisms are proposed to explain the cause of sintering [52]. The first one suggests that active metallic particles break free from the support and migrate to the surface. They coalesce and join with the other metals to form a bulky mass [53]. The second mechanism is a form of atom migration known as Oswald

ripening [54]. This process is one of the major reasons for deactivation of the catalyst. The driving factor is the difference in solubility between the small and large metallic particles. Large nanoparticles are formed by the addition of small nanoparticles by diffusion to reach a more stable thermodynamic state [55]. The particle size is governed by nucleation and kinetics. Nucleation is the addition of small nuclei particles to form bigger particles which add to the stability. But this reduces the surface area of the catalysts. This leads to the closure of pores because the metal particles get closely packed together forming a compact arrangement of metallic particles. Agglomeration process is promoted by the heating at elevated temperatures. When the small metallic particles come close together, they grow and agglomerate, and eventually bulky metal particles with low surface area start to appear as shown in Figure 10. Metals in general prefer to be packed as tightly as possible to maximize the packing factor. From a thermodynamic perspective, small active particles are less favored and they are unstable compared to big bulky tightly packed metallic particles. Provided with sufficient energy in the form of heat, the metals will rearrange to form larger particles that are incompetent with catalysis [56].

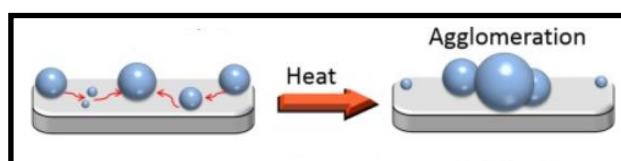


Figure 10: Agglomeration of Ni particles at high temperature [57]

2.6.2 Carbon Deposition

Carbon deposition has a considerable influence on the activity and stability of catalysts as a result of covering the active sites for the reaction. Two types of carbon deposition are observed in partial oxidation and other methane reforming reactions,

encapsulate carbon which envelops the Ni particles causing deactivation and whisker carbon, which accumulates on the face of the Ni particles. There are two mechanisms proposed for carbon formation. The first one is based on methane decomposition at high temperatures, where the dissociation of methane gives solid carbon and H₂ gas [3]. The second mechanism, which dominates at lower temperatures, is a redox reaction, first proposed by Octave Leopold Boudouard. This is called the Boudouard reaction, where CO disproportionation yields solid carbon and CO₂ gas [1]. All carbon-producing reactions are presented in Table 1.

Table 1: Proposed carbon-forming reactions [1]

$\text{CH}_4 \leftrightarrow \text{C} + 2\text{H}_2$
$2\text{CO} \leftrightarrow \text{C} + \text{CO}_2$
$\text{CO} + \text{H}_2 \leftrightarrow \text{C} + \text{H}_2\text{O}$
$\text{C}_m\text{H}_n \rightarrow \text{carbonaceous deposits}$

Chapter 3: Experimental Methods

3.1 Introduction

This chapter discusses the experimental procedures including the catalysts preparation method, catalytic activity tests, experimental setup, and materials characterization methods. The samples were characterized using X-ray powder diffraction (XRD), thermal gravimetric analysis (TGA), scanning electron microscopy (SEM), transmission electron microscopy (TEM), temperature programmed desorption (TPD), hydrogen temperature programmed reduction (H₂-TPR), CO chemisorption, and N₂ sorption. Alumina-supported Ni catalysts with different Ni concentrations were prepared and studied, including concentrations of 5%, 10%, 15% and 20% by mass. Three types of alumina-based support precursors were used in this study, namely γ -AlOOH, γ -Al₂O₃, and α -Al₂O₃. The catalysts were calcined at different temperatures ranging from 500-1100°C. The influence of the support precursor and the calcination temperature on different catalysts' characteristics as well as on their catalytic performance was investigated. The catalytic performance of the prepared catalysts were tested in the partial oxidation of methane reaction using a fixed-bed reactor.

3.2 Catalyst Preparation

Boehmite powder, γ -AlOOH, was purchased from Sasol Company. α -Al₂O₃ and Ni(NO₃)₂·6H₂O were obtained from Sigma-Aldrich. γ -Al₂O₃ was prepared by calcination of γ -AlOOH at 500°C for 4 hours. Supported Ni catalysts were prepared by wet impregnation of γ -AlOOH, γ -Al₂O₃, or α -Al₂O₃ with aqueous solutions of Ni(NO₃)₂·6H₂O. In a typical experiment, 1.0 g of γ -AlOOH or γ -Al₂O₃ was taken in

a ceramic crucible, to which around 1 mL of an aqueous solution containing the appropriate amount of $\text{Ni}(\text{NO}_3)_2 \cdot 6\text{H}_2\text{O}$ was added dropwise. In the $\gamma\text{-Al}_2\text{O}_3$ -derived catalysts, the support was calcined before impregnation at temperatures in the range of 500-1100°C. After impregnation, the obtained paste-like mixtures were aged for 24 hours, followed by drying in an oven at 120°C for 1 hour and calcination at 500°C for 4 hours. In addition, the $\gamma\text{-AlOOH}$ -derived catalysts were calcined after impregnation at temperatures in the range of 500-1100°C. Figure 11 presents images of a typical sample after the different preparation steps.

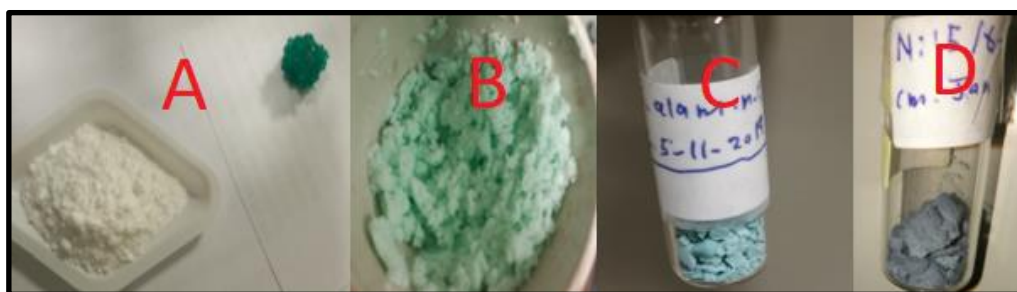


Figure 11: Images of a typical sample after the different preparation steps. (A) alumina support and nickel precursor, (B) impregnation, (C) $\text{Ni}/\gamma\text{-AlOOH}$ sample, (D) $\text{Ni}/\gamma\text{-Al}_2\text{O}_3$ sample.

After calcination, NiO is obtained on the support. Reduction in H_2 (10%) in He at 700°C was used to reduce NiO to Ni prior to reaction. In the catalysts where $\gamma\text{-AlOOH}$ was used as the support precursor, calcination after impregnation resulted in its complete conversion to $\gamma\text{-Al}_2\text{O}_3$. Depending on the calcination temperature after impregnation, the mixed oxide phase nickel aluminate NiAl_2O_4 also formed, as will be discussed below.

The $\gamma\text{-AlOOH}$ -derived catalysts are denoted as $\text{Ni}_x/\gamma\text{-AlOOH-y}$, and those based on pre-calcined $\gamma\text{-Al}_2\text{O}_3$ are denoted as $\text{Ni}_x/\gamma\text{-Al}_2\text{O}_3\text{-y}$, where “x” and “y”

represent the Ni loading (metal weight %) and the calcination temperature, respectively. Similarly, catalysts where the support is α -Al₂O₃ are denoted as Ni_x/ α -Al₂O₃-y. In Ni_x/ γ -Al₂O₃-y, the calcination temperature “y” refers to the calcination of the support before impregnation, noting that after impregnation the composites were calcined again at 500°C. In Ni_x/ γ -AlOOH-y, the calcination temperature “y” refers to the temperature of calcination after impregnation

3.3 Catalysts Characterization

The physiochemical properties of calcined and reduced catalysts as well as spent catalysts, after reactions, were characterized by various techniques including XRD, TGA, SEM, TEM, TPD, H₂-TPR, CO chemisorption, Raman Spectroscopy, CO adsorption by DRIFTS, and N₂ sorption. The results obtained from the different techniques showed significant dependence of the textural and structural properties on the support precursor as well as on the pre-treatment conditions.

3.3.1 X-ray Diffraction

Powder X-ray diffraction is a powerful, rapid and non-destructive technique used to evaluate catalysts. In this technique, X-rays are generated by a cathode ray tube, filtered and directed to the sample. The diffracted X-rays are detected and processed by a detector. Each particular phase of a crystalline solid consists of a specific atomic arrangement that produces a unique diffraction pattern. Therefore, every crystalline material has a unique diffraction pattern that distinguishes it from other materials. The output is a diffraction pattern presented as a plot of the intensity of X-rays scattered at different angles. The identification of phases is carried out by comparing the acquired experimental data to the reference database.

In the present research, XRD was employed to reveal the structure, the phase composition, and crystalline size of the prepared catalysts. XRD patterns were recorded on a Shimadzu-6100 powder XRD diffractometer with Cu-K α radiation, $\lambda = 1.542\text{\AA}$. Diffraction data were collected in the 2θ angle range of 20-80 deg. at a rate of 1 deg./min. Samples were well grinded and were placed on an aluminum sample holder. Crystalline sizes were calculated using Scherer equation shown below:

$$D = \frac{K\lambda}{\beta \cos\theta}$$

D - crystallite size, K - function of the crystallite shape, λ - X-ray wavelength, β - width of the X-ray diffraction peak, θ - Bragg angle

3.3.2 H₂-Temperature Programmed Reduction

H₂-TPR is a useful technique used to evaluate the reducibility of metal oxides in the pure form or dispersed over a support. In addition, it gives insights regarding the strength of interaction between the active phase and the support. Reduction that takes place at relatively low temperatures indicates reduction of a metal oxide with weak metal-support interaction. Conversely, reduction observed at high temperatures indicates the reduction of a species with strong metal-support interaction. Reducibility is also related to the particle size. As a general trend, particles of smaller sizes are easier to reduce as opposed to large particles which tend to reduce at a higher temperature because the core is not well exposed to the reducing agent, which is usually hydrogen. Also, the hydrogen diffusion rate is considerably slower in large particles due to the low permeability within the particles.

In a typical H₂-TPR experiment, hydrogen gas, the reducing agent is allowed over the sample as the temperature is gradually increased from room temperatures to

elevated temperatures, as high as 1000°C. The hydrogen uptake is usually measured by a thermal conductivity detector, already calibrated for hydrogen, and the TPR profile is represented as H₂ consumption as a function of temperature.

H₂-TPR was performed on a ChemBET-TPR/TPD chemisorption instrument from Quantachrome, USA. Samples (50 mg) were packed between two quartz wool plugs in a U-shaped quartz tube reactor and were degassed at 350°C for 1 hour, under N₂ flow at 30 mL/min. After cooling to 25°C, the reducing gas, 5% H₂ in N₂, was allowed over the sample at a rate of 50mL/min while heating at 10 deg./min up to 950°C. The H₂ uptake was measured by a thermal conductivity detector.

3.3.3 Thermogravimetric Analysis

Thermogravimetric analysis (TGA) is a thermal characterization method that monitors the mass of a sample as a function of temperature. It is a complementary technique used with other characterization methods to verify the identity of a certain material. It is employed to characterize polymers, ceramics, glasses and composite materials. In addition, it can be used to determine water or residual content in materials via thermal decomposition in air and evaporation. Thermogravimetric analysis can confirm the findings of XRD patterns regarding the phase compositions because there is a strong correlation between phase composition and thermal stability. The mass of the studied sample is monitored continuously during the experiment. The amount of weight loss provides information about the thermal stability and phase composition of the catalyst. These properties of the catalysts are usually governed by the preparation method, calcination temperature and metal-support interactions.

In the present work, TGA was used to measure the amount of carbon deposits on spent catalysts. In a typical experiment, approximately, 3 mg of the catalyst was

loaded in an aluminum pan as shown in Figure 12. The pan was heated in air from 25 to 600°C by an electrical furnace at a rate of 20 deg./min. The sample temperature was then held at 600°C for additional one hour to achieve complete carbon combustion and removal.

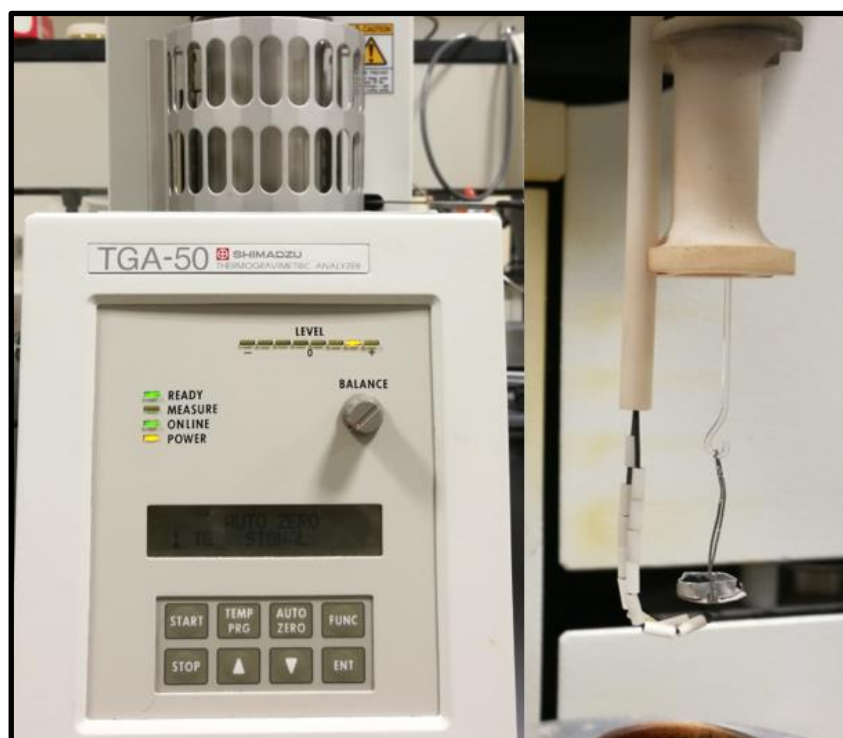


Figure 12: TGA instrument

3.3.4 Nitrogen-Sorption Analysis

N₂-sorption at the liquid N₂ temperature (77K) is a common technique used for surface area measurement and pore characterization of solids. The extent of adsorption on the surface depends on the N₂-relative pressure (P/P_0). Increasing the pressure of N₂ over the sample causes an increase in the amount of adsorption, which starts on the external surface as a monolayer of N₂ molecules followed by condensation in the pores. After saturation, desorption starts, which is inversely proportional to the

pressure. N₂ sorption analysis results are presented in an isotherm, which is a plot of the number of adsorbed molecules as a function of the relative pressure.

In the present study, N₂ sorption was conducted at 77K using a TriStar-II volumetric gas sorption instrument from Micrometrics. Before measurements, samples were degassed at 200°C for 2 hours under vacuum. Specific surface areas were determined by Brunauer-Emmett-Teller (BET) theory, and pore size distributions were determined by the Barrett-Joyner-Halenda (BJH) model based on the desorption branch of the N₂ isotherms.

3.3.5 CO Pulse Chemisorption

CO chemisorption is a useful technique that allows measuring the active metal surface area, metal dispersion, and crystallite size. Metal dispersion is a ratio of the overall metallic atoms on the surface accessible to the adsorbate species compared to the total number of metallic atoms present in the sample. In other words, the total number of CO molecules adsorbed as a ratio to the total number of Ni metallic particles present in the sample. Since CO molecules adsorb selectively on the active metal atoms, the number of adsorbed molecules can be used to determine the metallic surface area (m²/g metal) and active metal crystallite size.

In the present study, CO chemisorption was carried out on the same instrument used for the H₂-TPR experiments. Samples of 75 mg were packed in a quartz tube and were pre-treated under He (50 mL/min) at 700°C for 1 hour followed by reduction at the same temperature for 2 hours using 5% H₂ in N₂ at a flow rate of 50 mL/min. The samples were then cooled to 30°C at which pure CO pulse titration was carried out. The amount of adsorbed CO was determined by a thermal conductivity detector, which was calibrated for CO under the same conditions.

3.3.6 TEM and SEM Analysis

Transmission electron microscopy (TEM) is widely used for the characterization of catalysts' morphology. The catalyst is bombarded with a high energy beam of electrons. The interaction of the electron beam with the crystal structure of the sample yields information about the identity of the phase, particle size, and the homogeneity of the metal distribution. SEM creates images by detecting reflected or scattered electrons from the sample, giving information about the surface topology. TEM offers superior spatial resolution and more information compared to SEM. In this study, TEM images were obtained using a CM10 Philips electron microscope, where ethanol suspensions of the samples were deposited on a carbon film attached to a copper grid. SEM images were obtained using a Thermo-Fisher Quattro S electron microscope, where samples were prepared using the same method used in TEM.

3.3.7 CO₂ and NH₃-TDP

Temperature programmed desorption (TPD) of probe molecules allows for studying different chemical properties of solid surfaces including acidic and basic characteristics. The desorption profile of the adsorbed molecules reveals information about the extent of adsorption and the strength of binding with the surface. A thermal conductivity detector is very often used for measuring the amount of the desorbed molecules. NH₃ is a basic substance that adsorbs on acidic sites, and therefore, it is commonly used as a probe molecule to measure the total surface acidic sites. The area of the desorption peak represents the number of surface acidic sites and the peak temperature represents the strength of the individual sites. CO₂, on the other hand, is used as a probe molecule to characterize surface basic sites. NH₃ and CO₂ have small

molecular sizes allowing them to penetrate the pores of the sample. After saturating the solid sample with the adsorbate molecules at room temperature, the sample is heated gradually to elevated temperatures, and the amount of the desorbed gas is monitored versus temperature. Peaks of desorption at low temperatures represent weak acidic or weak basic sites, depending on the adsorbed probe, and those at high temperatures correspond to strong sites.

In the present work, CO₂ and NH₃-TPD studies were performed on the same chemisorption instrument, ChemBET-TPR/TPD from Quantachrome. Reduced samples of 120 mg were packed in a U-shaped quartz tube reactor and were degassed at 350°C for 1 hour, under He flow of 50 mL/min. The samples were reduced again in situ at 750°C for 1 hour using 5% H₂ in N₂ at a flow rate of 50 mL/min. After cooling to 30°C, CO₂ or NH₃ was allowed to flow through the samples at a rate of 40 mL/min for adsorption. The samples were then purged at 30°C for 20 min to remove the gas phase and the physically adsorbed molecules before ramping the temperature to 850°C at a rate of 10 deg./min under He flow at 50 mL/min. The amount of the desorbed gas was recorded during the heating process by a TCD detector.

3.4 Catalytic Study

A scheme of the experimental system employed in the catalytic activity tests is shown in Figure 13. The system consists of the following: three mass flow controllers to control and monitor the flow rate of gases, a stainless steel tubular system to allow gas flow, a quartz tube reactor, an electric heater, an ice trap to condense water, a pressure gauge, and a 6-way sampling valve to allow direct injection of the gaseous products into a gas chromatograph, GC. The GC was connected in-line with the reaction set-up and was equipped with a TCD detector.

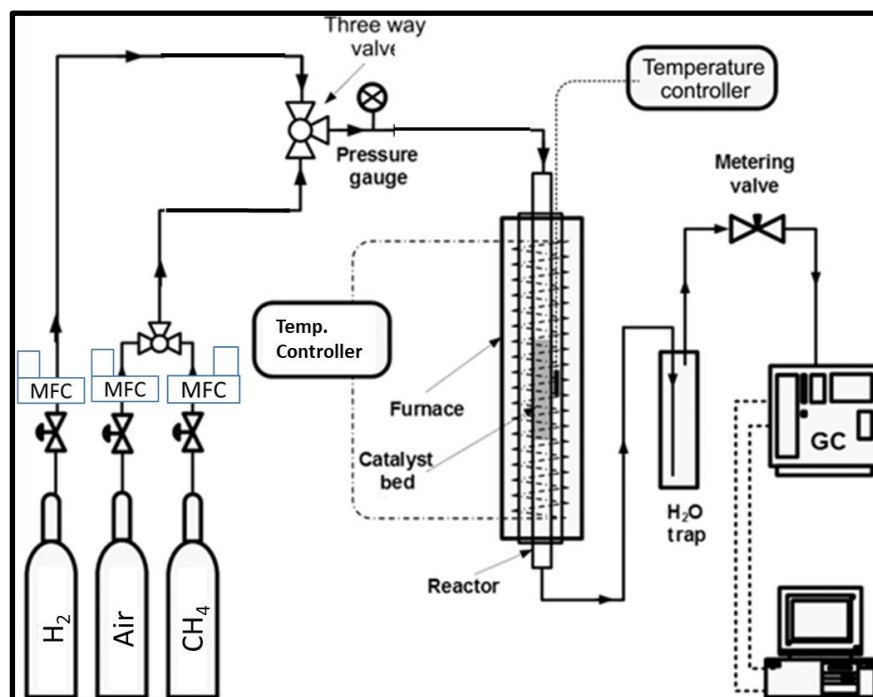


Figure 13: schematic diagram of the catalytic reaction setup

Catalytic activity tests were carried out at 700°C under atmospheric pressure where the reactants were allowed to continuously flow through a fixed bed of the catalyst in the quartz tube reactor. In a typical experiment, 1.2 g of catalyst (180-350 μm granules) was packed between two quartz wool plugs in the reactor tube, which was of 40 cm in length and had a 9 mm inside diameter. The quartz reactor tube was placed into a vertical electrical tube furnace equipped with a k-type thermocouple placed in the catalyst bed and a temperature controller to regulate the temperature. The catalysts were oxidized in-situ using air at 550°C for 15 min, followed by reduction at 700°C for an hour using a mixture of 8% H_2 in N_2 before starting the reaction. The reaction feed was composed of CH_4 (30%), O_2 (15%) and N_2 (55%) with a total flow rate of 50 mL/min. The reaction was started by introducing air and methane mixture, which were allowed through a by-pass line for 5 min for premixing. The products were analyzed twice during the first hour of reaction and every one hour after that for

a total of 45 hours using a 6-way valve for direct sampling into the GC. A cold trap of ice was used to trap and condense the water vapor formed during the reaction. The GC was calibrated for all gases involved to enable measuring the concentration of the reactants and the products. The catalysts after the reaction were characterized by powder XRD, TGA and Raman Spectroscopy to identify structural changes and measure and characterize carbon deposits. The CH₄ conversion and product selectivity were calculated according to the equations shown, where *MF* refers to molar flow rate:

$$CH_4 \text{ Conversion (\%)} = \frac{MF(CH_4)_{in} - MF(CH_4)_{out}}{MF(CH_4)_{in}} \times 100$$

$$H_2 \text{ Selectivity (\%)} = \frac{MF(H_2)}{2(MF(CH_4)_{in} - MF(CH_4)_{out})} \times 100$$

$$CO \text{ Selectivity (\%)} = \frac{MF(CO)}{MF(CH_4)_{in} - MF(CH_4)_{out}} \times 100$$

$$CO_2 \text{ Selectivity (\%)} = \frac{MF(CO_2)}{MF(CH_4)_{in} - MF(CH_4)_{out}} \times 100$$

Chapter 4: Results and Discussion

4.1 Structural Characterization

The type of Ni species in the prepared catalysts before reduction was greatly dependent on the structure of the support precursor before impregnation and on the calcination temperature. The catalysts prepared from impregnated γ -Al₂O₃, precalcined at different temperatures, always contained a mixture of NiO and NiAl₂O₄ as shown in Figure 14. In addition, their XRD patterns showed that γ -to θ -Al₂O₃ transformation started around 850°C as indicated by the distinct peaks that started to appear at 2θ of 32.7° and 38.5°. When γ -AlOOH was impregnated with the Ni precursor first, then calcined at different temperatures, NiO was the dominant Ni species after calcination at 500°C, which decreased at 650°C, as shown in Figure 15A. However, NiO peaks disappeared completely upon calcination at temperatures $\geq 750^\circ\text{C}$ indicating a complete reaction with the alumina support forming NiAl₂O₄ as the main Ni species at elevated temperatures. It is also noteworthy that γ - to θ -Al₂O₃ transformation was not seen in these catalysts at temperatures as high as 950°C, while such transformation was clearly observed at this temperature in the catalysts based on precalcined γ -Al₂O₃ support, as presented in Figure 14. Such phase transformation was observed by XRD only after calcination at temperatures $\geq 1050^\circ\text{C}$, not shown. The resistance of γ -Al₂O₃ to structural changes in the case of γ -AlOOH-derived catalysts can be referred to the presence of significant amounts of NiAl₂O₄ upon calcination at elevated temperatures, which may have hindered such transformation.

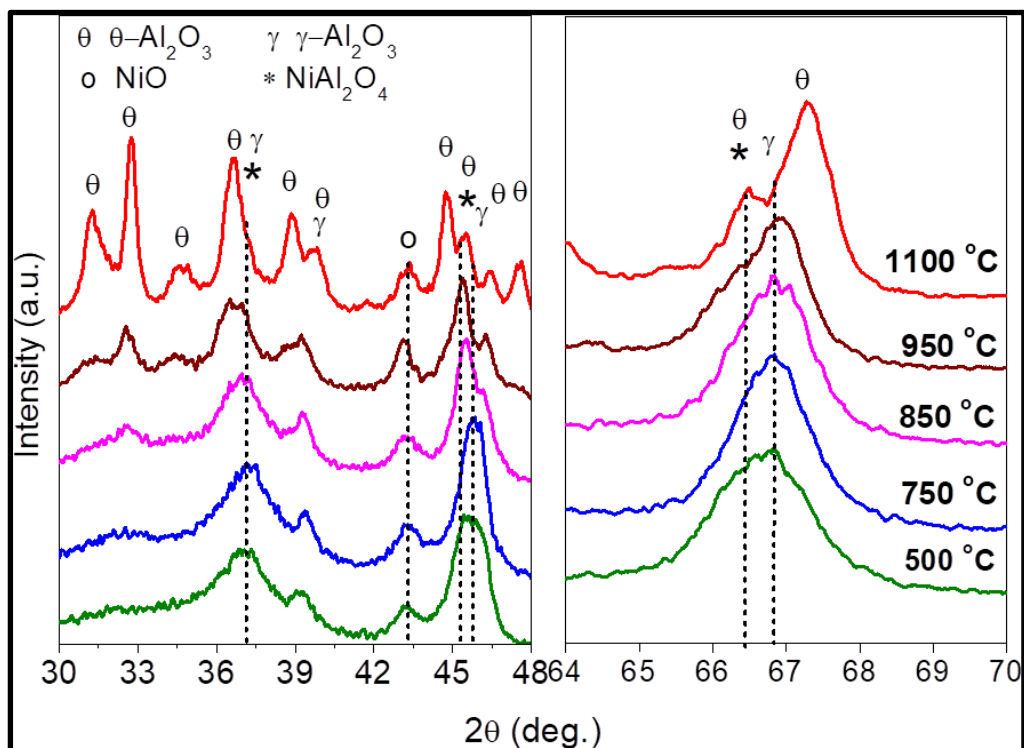


Figure 14: X-ray diffraction (XRD) patterns of Ni/ γ -Al₂O₃ catalysts.

The XRD patterns of γ -Al₂O₃ and NiAl₂O₄ significantly overlap, due to similar lattice parameters, which are 7.894 and 8.053 Å for γ -Al₂O₃ and NiAl₂O₄, respectively [58,59]. However, the formation of NiAl₂O₄ is indicated by the noticeable increase in the intensity of the peak at 2θ of 37°, and a small shift of the peaks at 2θ of 46° and 67° to lower values as clearly shown in the inset of Figure 15A. The stoichiometric NiAl₂O₄ spinel usually shows diffraction peaks at 2θ values of 19°, 31.4°, 37°, 45°, 59°, and 65.5° [60]. Small shifts in the peaks of NiAl₂O₄ in the prepared composites to slightly higher values may indicate nonstoichiometric NiAl₂O₄.

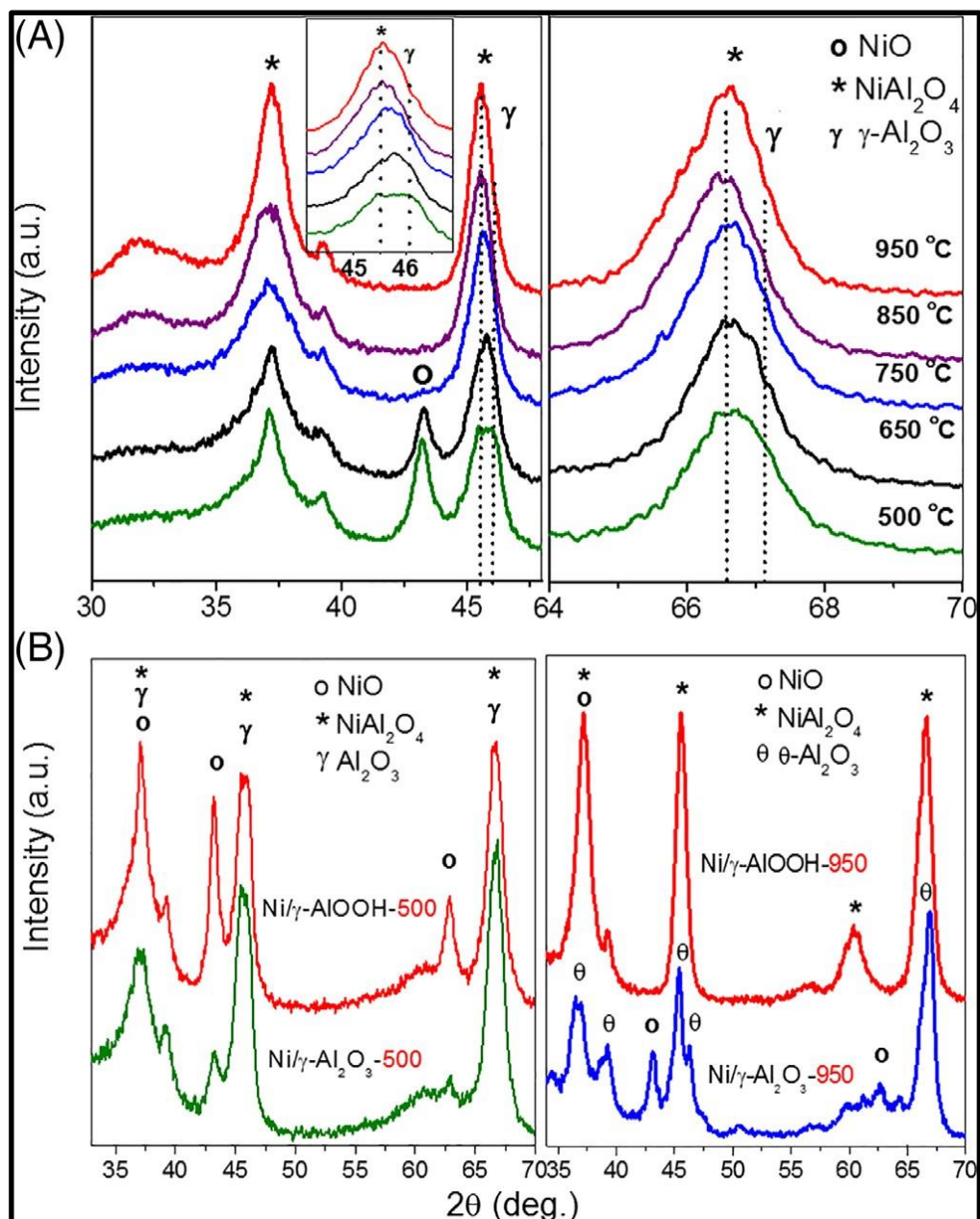


Figure 15: X-ray diffraction (XRD) patterns of (A) Ni/ γ -AlOOH catalysts calcined after impregnation at temperatures (B) Ni/ γ -AlOOH-500 and Ni/ γ -AlOOH-950 compared with their counterparts based on γ -Al₂O₃.

The variations in the composition of the catalysts from both preparation routes can be more easily seen in the comparisons presented in Figure 15B. Comparing Ni/ γ -AlOOH-500 and Ni/ γ -Al₂O₃-500 shows that NiO formed in a larger amount, on the account of NiAl₂O₄, in Ni/ γ -AlOOH-500, which may be inferred from its significantly

more intense peaks. These observations indicate that the NiO-support interactions are strongly dependent on the support and on the calcination temperature, which may indicate weaker interactions in Ni/ γ -AlOOH-500 as evident from the dominance of crystalline NiO on its surface. However, this interaction trend is reversed at elevated temperatures as shown in Figure 15B at 950°C. These results were well supported by H₂-TPR and CO chemisorption studies as will be discussed below. Compared to γ -AlOOH and γ -Al₂O₃-derived catalysts, the pattern of α -Al₂O₃-supported catalysts showed highly crystalline NiO as the sole Ni species before reduction, which indicates weaker interactions with the crystalline α -Al₂O₃ support. The XRD patterns of the catalysts after reduction at 700°C are shown in Figure 16. The patterns of Ni/ γ -Al₂O₃ catalysts (Figure 16A) showed peaks for Ni and NiAl₂O₄, besides peaks for θ -Al₂O₃ at 950°C, confirming the phases observed before reduction shown in Figure 14. The patterns of reduced γ -AlOOH-derived catalysts in (Figure 16B) showed the enhanced formation of Ni at moderate calcination temperatures (500-650°C) which correlates with the observed favored formation of NiO on their surfaces on the account of NiAl₂O₄ before reduction. Calcination at higher temperatures enhanced the interaction with the support resulting in less Ni as indicated by the observed decrease in its peaks, until it disappeared completely at 950°C, where hard to reduce NiAl₂O₄ was observed as the sole Ni species.

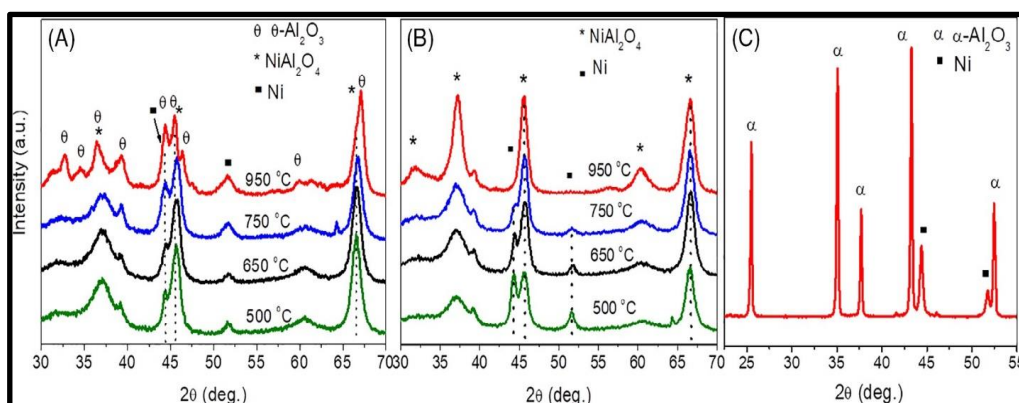


Figure 16: X-ray diffraction (XRD) patterns of reduced Ni catalysts over (A) γ - Al_2O_3 (B) γ - AlOOH and (C) over α - Al_2O_3 .

Figure 16 also presents the diffraction pattern of reduced Ni/ α - Al_2O_3 , which shows the presence of crystalline Ni particles as the sole Ni species confirming the weak interaction with the support suggested above. These results suggest that using γ - AlOOH as a precursor for the support of Ni followed by moderate calcination, at a temperature around 650°C , is a promising route for the synthesis of more reducible Ni catalysts. The enhanced formation of NiO, before reduction, on moderately calcined γ - AlOOH -derived catalysts may be referred to the fact that the surface of γ - AlOOH is rich of hydroxyl groups, distributed evenly on its surface, to which the Ni^{2+} ions adsorb and coordinate during impregnation. Upon calcination at moderate temperatures, γ - AlOOH converts to γ - Al_2O_3 with a significant amount of the OH groups retained on its surface with which the adsorbed Ni ions react to produce NiO on the account of the reaction with the support lattice.

4.2 Catalysts' Reducibility

Figure 17A shows the H₂-TPR profiles of γ -AlOOH- and γ -Al₂O₃-based catalysts calcined at 500°C and 650°C as well as that of Ni/ α -Al₂O₃. Supported NiO usually shows reduction in the temperature range of 400°C to 750°C, depending on the strength of its interaction with the support [61, 62]. The profile of Ni/ α -Al₂O₃ showed a reduction peak centered around 500°C, which is a typical reduction profile for NiO particles weakly bound to the support. It also showed no indication of the presence of NiAl₂O₄, which usually shows reduction at temperatures >900°C [63].

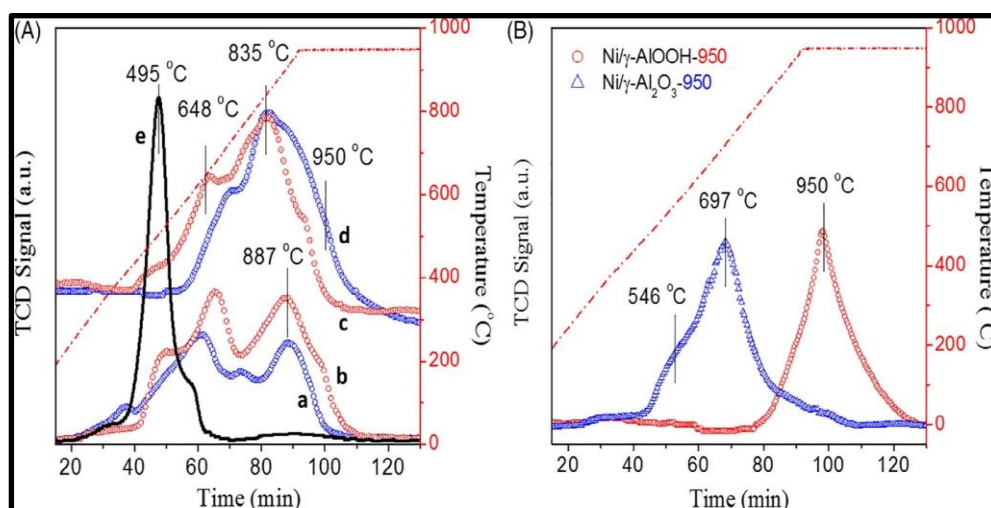


Figure 17: H₂-TPR profiles of selected catalysts. A, (a) Ni/ γ -Al₂O₃-500 (b) Ni/ γ -AlOOH-500 (c) Ni/ γ -AlOOH-650 (d) Ni/ γ -Al₂O₃-650 (e) Ni/ α -Al₂O₃. B, Ni/ γ -Al₂O₃-950 and Ni/ γ -AlOOH-950.

The γ -AlOOH and γ -Al₂O₃-based catalysts calcined at 500°C showed different overlapping reduction peaks over a wide temperature range that can be divided into three main regions. First, reduction in the low temperature range, 450°C to 600°C, which represents weakly bound NiO to the support. The second region between 600°C and 700°C refers to the reduction of NiO that binds more strongly to the surface. The

third reduction region in the profile, 750°C to 950°C, can be referred to NiO that binds very strongly to the support, in addition to NiAl₂O₄ phase. It is evident that Ni/ γ -AlOOH-500 showed a higher degree of reduction as indicated by the larger area under its peaks, which represent the amounts of H₂ consumed during the reduction process as presented in Table 2. These results agree with the XRD results of the reduced catalysts in Figure 16 that indicated more NiO on Ni/ γ -AlOOH-500 compared to Ni/ γ -Al₂O₃-500. The profiles of the catalysts calcined at 650°C closely resembled their counterparts treated at 500°C, except that in both types of catalysts, the high-temperature reduction increased on account of that at low temperatures, which can be a consequence of thermally enhanced NiO-support interactions. The difference in the behavior of the two types of catalysts presented in Figure 17A can be explained to the different properties of the γ -AlOOH surface that allowed for better dispersion of NiO particles as was confirmed by CO chemisorption, as discussed in Figure 17B shows the reduction profiles of the two types of catalysts treated at 950°C. Ni/ γ -AlOOH-950 showed reduction at high temperatures only as indicated by a peak centered at 950°C indicating the presence of NiAl₂O₄ as the sole Ni species, which agrees with its XRD pattern that was recorded after reduction, Figure 3, where only NiAl₂O₄ was detected. However, the profile of Ni/ γ -Al₂O₃-950 showed reduction over a wide temperature range (500°C-800°C) with a major peak centered around 700°C indicating the dominance of NiO, with relatively strong interaction with the support. The absence of significant reduction >850°C, where only a weak shoulder was observed, indicates the absence of significant amounts of NiAl₂O₄. In addition, the hydrogen uptake by Ni/ γ -Al₂O₃-950 was noticeably higher than that of Ni/ γ -AlOOH-950 as shown in Table 2, which agrees with the known lower reducibility of NiAl₂O₄ that was detected as the sole Ni phase in this catalyst. Comparing the profile of Ni/ γ -Al₂O₃-950 with that of

Ni/ α -Al₂O₃ (Figure 17A) shows that the NiO interactions with θ -Al₂O₃ (which is the main support phase in Ni/ γ -Al₂O₃-950) are stronger than in the case of α -Al₂O₃, where the reduction took place at significantly lower temperature. The effect of the temperature on the reducibility was dependent on the support precursor. For the γ -Al₂O₃-based catalysts, the hydrogen uptake noticeably increased when the calcination temperature of the support was increased from 500°C to 650°C, as shown in Table 2. The lower reducibility of Ni/ γ -Al₂O₃-500 could be explained to the fact that γ -Al₂O₃ has a metastable structure, and when calcined at 500°C, it is usually amorphous or weakly crystalline with relatively large pore volume [64] which was confirmed by the N₂ sorption results as shown in Table 3.

Table 2: Hydrogen consumption during H₂-temperature programmed reduction (H₂-TPR)

Sample name	H ₂ uptake ($\mu\text{mol g}^{-1}$)
Ni/ γ -Al ₂ O ₃ -500	837.8
Ni/ γ -AlOOH-500	995.1
Ni/ γ -Al ₂ O ₃ -650	974.8
Ni/ γ -AlOOH-650	970.3
Ni/ α -Al ₂ O ₃	601.2
Ni/ γ -Al ₂ O ₃ -950	785.6
Ni/ γ -AlOOH-950	654.5

Table 3: Brunauer-Emmett-Teller (BET) surface area and pore characteristics of the reduced catalysts

Composition	$S_{\text{BET}}^{\text{a}}$ ($\text{m}^2 \text{g}^{-1}$)	TPV ^b ($\text{cm}^3 \text{g}^{-1}$)	APD ^c (nm)
γ -AlOOH	89.5	0.45	19.1
γ -Al ₂ O ₃	132.8	0.80	25.4
Ni/ γ -Al ₂ O ₃ -500	100.6	0.71	25.5
Ni/ γ -AlOOH-500	124.3	0.56	19.3
Ni/ γ -Al ₂ O ₃ -650	91.7	0.50	22.1
Ni/ γ -AlOOH-650	100.1	0.49	19.4
Ni/ γ -Al ₂ O ₃ -750	83.5	0.51	23.0
Ni/ γ -AlOOH-750	96.9	0.49	22.4
Ni/ γ -Al ₂ O ₃ -950	67.6	0.80	34.9
Ni/ γ -AlOOH-950	80.1	0.48	23.0
Ni/ α -Al ₂ O ₃	6.0	0.018	23.9

a) BET-specific surface area. b) TPD is the total pore volume c) APD, average pore diameter.

Impregnation of γ -Al₂O₃ precalcined at this temperature, may result in some NiO particles in the pores, and during the reduction process at elevated temperatures considerable sintering of the support takes place, which may lead to confinement of some of these particles in closed pores, and hence to less exposure. On the other hand, when the support was precalcined at 650°C, it became more texturally stable, where more NiO would be on the external surface of the support particles leading to easier reduction. In addition, the effect of reduction conditions on the textural properties would be less severe. This explanation becomes more reasonable when noting that the loss in the surface area was <10% upon increasing the calcination temperature of the support to 650°C, while the pore volume decreased from 0.8 to 0.5 cc g⁻¹, representing a drop of close to 40%, as shown in Table 3. When the calcination temperature of the support was increased to 950°C, the hydrogen uptake decreased noticeably. While this

behavior is still not well understood, it may be related to the significant structural transformation of the support from γ - Al_2O_3 to θ - Al_2O_3 , as was confirmed by XRD, which may also indicate stronger interaction of the Ni particles with the support. The γ - AlOOH -derived catalysts showed a different trend in the H_2 -uptake vs the calcination temperature. The hydrogen consumption was relatively high for both catalysts calcined at 500°C and 650°C , which correlates with the weaker Ni-support interactions suggested in the XRD discussion above, and correlates with the enhanced dispersion of Ni particles in these catalysts, as confirmed by the CO chemisorption. The H_2 consumption decreased considerably upon calcination at 950°C , which can be referred to the observed complete NiO-support reaction that resulted in hard to reduce NiAl_2O_4 , as was confirmed by the XRD results.

4.3 Textural and Morphological Properties

All prepared catalysts showed relatively high surface areas and large total pore volumes that were retained, to a good degree, upon calcination at elevated temperatures as shown in Table 3. γ - Al_2O_3 , obtained from calcination of γ - AlOOH at 500°C , showed higher surface area and larger pore volume compared to γ - AlOOH . However, all Ni/ γ - AlOOH -derived catalysts showed noticeably higher surface areas and, generally, lower total pore volumes than their counterparts based on precalcined γ - Al_2O_3 . The higher surface areas could be referred to the presence of the Ni species during calcination hindering, to some extent, sintering of the support. The slight decrease in the total pore volume and the average pore diameter indicates the formation of smaller primary particles resulting in smaller interparticle pores upon aggregation, which also correlates with the increase in the surface areas. Ni/ α - Al_2O_3 , on the other hand, possessed very low surface area and negligible porosity due to the highly

crystalline nature of the support. TEM and SEM images as well as elemental mapping of selected reduced catalysts are shown in Figure 18.

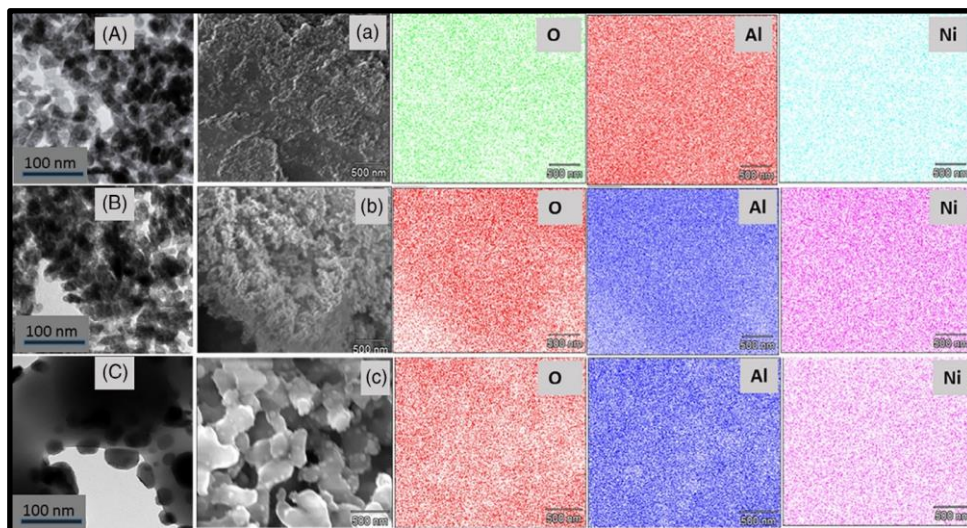


Figure 18: TEM, A-C, and SEM, a-c images of reduced Ni/ γ -AlOOH-650, A,a, Ni/ γ -Al₂O₃-650, B,b, and Ni/ α -Al₂O₃, C,c. SEM, scanning electron microscopy; TEM, transmission electron microscopy.

The images of Ni/ γ -AlOOH-650 and Ni/ γ -Al₂O₃-650 showed Ni nanoparticles with sizes in the range of 15 to 30 nm. However, the image of Ni/ α -Al₂O₃ showed larger crystals of Ni with diameters between 20 and 60 nm. Crystallite sizes and other textural properties of the Ni particles were also characterized by CO chemisorption, as discussed next, where the results showed a good agreement with the TEM images.

SEM images of Ni/ γ -AlOOH-650 and Ni/ γ -Al₂O₃-650 showed highly aggregated primary particles. Such aggregation of small particles creates a significant amount of mesopores that lead to high surface areas, which agrees with the textural properties shown in Table 3. In such textures, the Ni species are expected to disperse on the external surfaces and to condense inside the mesopores. However, Ni/ α -Al₂O₃, which had negligible porosity, showed large crystals of the support with the Ni

particles dispersed on the external surface. The elemental mapping associated with the SEM images showed evenly distributed Ni throughout the catalysts.

4.4 CO Pulse Chemisorption

Active metal dispersion, surface area, and crystallite size were characterized by CO chemisorption on the reduced catalysts at room temperature, and the results are presented in Table 4. The % dispersion values for all catalysts were in the range of 1.0 to 3.4, which are reasonable values, given the high metal loading employed. Interestingly, Ni/ γ -AlOOH-650 showed noticeably higher dispersion, larger metal surface area, and smaller Ni crystallites compared to Ni/ γ -Al₂O₃-650 and the other catalysts.

Table 4: Metal dispersion, surface area, and crystallite size

Catalyst	Metal dispersion (%)	Metallic surface area (m ² g ⁻¹ metal)	Active metal crystallite size (nm)	Crystallite size based on XRD (nm)
Ni/ γ -Al ₂ O ₃ -500	1.6	10.8	31.2	25.6
Ni/ γ -AlOOH-500	2.3	15.3	21.9	22.4
Ni/ γ -Al ₂ O ₃ -650	1.7	11.4	29.6	24.1
Ni/ γ -AlOOH-650	3.4	22.4	15.0	16.4
Ni/ γ -Al ₂ O ₃ -950	2.3	15.3	22.0	23.1
Ni/ γ -AlOOH-950	2.5	16.9	18.9	15.2 ^a
Ni/ α -Al ₂ O ₃	1.0	6.4	52.6	43.9

a) The crystallite size of NiAl₂O₄, which was the sole Ni phase in Ni/ γ -AlOOH-950 detected by X-ray diffraction (XRD).

These properties of Ni/ γ -AlOOH-650 correlate with its enhanced reducibility at lower temperatures observed by H₂-TPR. The lower dispersion values for the catalysts treated at 500°C can be referred to the expected thermal instability of the structurally metastable support,

which would result in some restructuring and more severe sintering during the reduction step conducted before the CO adsorption. The difference between Ni/ γ -AlOOH-650 and its counterpart, Ni/ γ -Al₂O₃-650, can be explained by the different surface properties of the γ -AlOOH support precursor compared to γ -Al₂O₃ as discussed below. The decrease in the Ni dispersion in Ni/ γ -AlOOH-950 can be explained by the high calcination temperature, which resulted in sintering and reaction of Ni species with the support leading to the formation of crystalline NiAl₂O₄ phase, as confirmed by XRD. The low dispersion over α -Al₂O₃ can be explained by its highly crystalline nature and very low surface area. The enhanced dispersion in Ni/ γ -AlOOH-650 can be explained by the surface characteristics of the support precursor, γ -AlOOH, compared to γ -Al₂O₃ surface, which are presented schematically in Figure 19. γ -Al₂O₃ has a cubic defect spinel structure, where oxygen ions adopt a cubic close packing arrangement and Al ions occupy octahedral and tetrahedral interstitial holes, with vacant Al sites distributed throughout the structure [64].

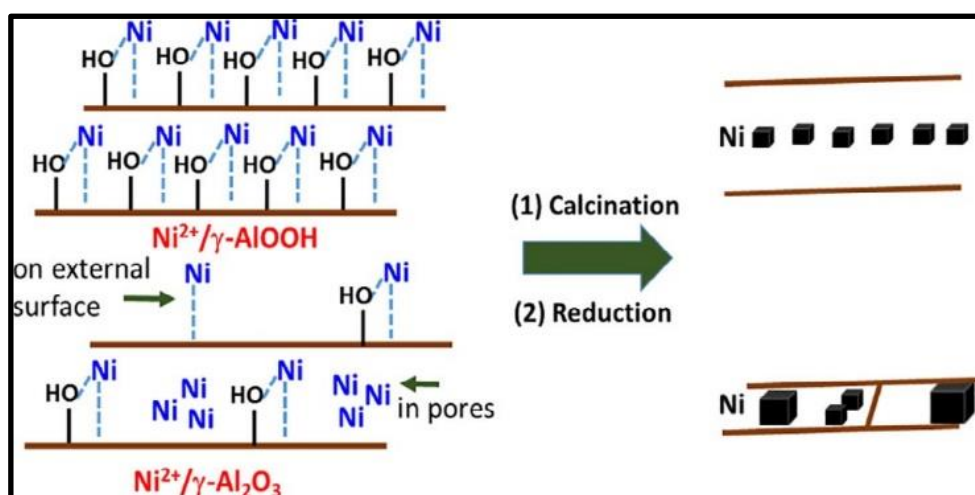


Figure 19: Schematic representation of the effect of the surface properties of the support precursor on the textural properties of the Ni particles.

Coordinatively unsaturated Al ions on the surface are stabilized by adsorbed species, especially hydroxyl groups that are weakly acidic. Dehydroxylation upon treatment at high temperatures results in unsaturated cationic sites on the surface that, along with the oxide sites, exhibit acid-base properties. Therefore, the concentration and the type of surface hydroxyl groups, as well as the coordination of the surface sites depend on the pretreatment conditions. On the other hand, γ -AlOOH has an orthorhombic structure where the unit cell consists of two double layers of aluminum-centered distorted $\text{AlO}_4(\text{OH})_2$ octahedra [65]. Hydroxyl groups are located at the outer surface of the double layers and interact through hydrogen bonding to hold the layers together. Therefore, compared to γ - Al_2O_3 , γ -AlOOH possesses a more homogeneous surface terminated with hydroxyl groups, as shown in Figure 19. In addition, while γ - Al_2O_3 surface is acidic in character, the surface of γ -AlOOH is basic, as has been reported using different surface characterization techniques [65]. Three types of basic sites were identified on the surface of γ -AlOOH including surface OH groups, coordinatively saturated oxide ions, and coordinatively unsaturated oxide ions, which are the most basic. We believe that the basic nature of γ -AlOOH surface enhanced adsorption of the Ni ions on the external surface through Lewis acid (Ni^{2+})-base (surface basic sites) interactions. This enhanced Ni-support interactions with the homogeneously distributed surface basic sites minimized sintering of Ni particles on the external surface as well as aggregation in the inter-particle pores of the support. In addition, homogeneous dispersion of the Ni species on the surface minimized sintering of the support particles, which is confirmed by the observed higher surface areas of these catalysts compared to their γ - Al_2O_3 -derived counterparts, Table 3.

4.5 CO₂ and NH₃ TPD

Acid-base properties of the catalysts were characterized by CO₂- and NH₃-TPD. Figure 20 shows the TPD profiles, and Table 5 displays the total acidic and basic site densities. While the catalysts showed some variations in the basic site strength and distribution (Figure 20A), three general desorption temperature ranges can be identified. The first desorption peak centering at a temperature around 120°C is common in the profiles of all catalysts. This peak is usually referred to desorption of CO₂ from weak basic sites that are believed to be basic OH groups [66]. The second desorption in the temperature range of 200°C to 400°C can be referred to medium strong basic sites, which are believed to be surface O²⁻ ions. In addition, some samples showed desorption at temperatures >600°C, indicating the presence of some very strong basic sites, which could be coordinatively unsaturated surface O²⁻ ions [64]. This feature is more pronounced in the profile of pure γ -Al₂O₃, and disappeared or became negligible in the profiles of the catalysts, which can be explained by the anticipated coverage of such sites by the Ni particles that are acidic in nature. Interestingly, basic site density and distribution showed noticeable dependence on the type of the support precursor and the calcination temperature. Comparison between both types of catalysts treated at 500°C and 650°C shows that the catalysts derived from Ni/ γ -AlOOH possessed noticeably higher basic site density compared to their counterparts based on Ni/ γ -Al₂O₃. These results correlate well with the reported basic nature of γ -AlOOH compared to γ -Al₂O₃, where some basic OH groups seemed to be retained upon calcination [64]. It is also note-worthy that Ni/ γ -AlOOH-650 showed the highest syngas selectivity in the POM reactions as discussed below, which may indicate a role of such sites in the reaction mechanism. The two catalysts treated at

950°C showed profiles different from those of the other catalysts, and from the typical Ni/ γ -Al₂O₃ profile [67]. This can be related to the considerable structural changes associated with this treatment temperature, where the support of Ni/ γ -Al₂O₃-950 became, mainly, θ -Al₂O₃, and the sole Ni species in Ni/ γ -AlOOH-950 was confirmed to be NiAl₂O₄. Ni/ α -Al₂O₃ showed the lowest amount of desorbed CO₂, which can be referred to its highly crystalline structure with very low surface area. The NH₃-TPD profiles (Figure 20B) showed major NH₃ desorption in the temperature range of 100°C to 300°C indicating the dominance of acidic sites of weak-medium strength [67].

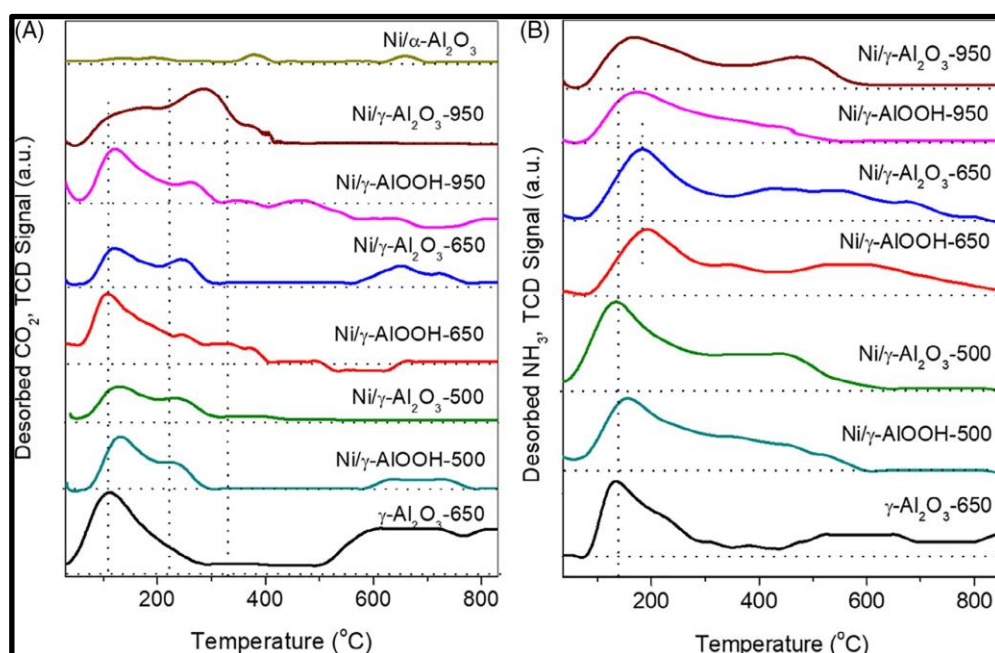


Figure 20: CO₂-TPD (A) and NH₃-TPD (B) profiles of the catalysts and pure γ -Al₂O₃. TPD, temperature-programmed desorption.

Table 5: Total acidic sites and basic sites of catalyst and pure γ -Al₂O₃

Samples	Basic site density		Acidic site density		Base/acid ratio
	$\mu\text{mol g}^{-1}$	$\mu\text{mol m}^{-2}$	$\mu\text{mol g}^{-1}$	$\mu\text{mol m}^{-2}$	
γ -Al ₂ O ₃	36.9	0.28	108.3	0.81	0.34
Ni/ γ -Al ₂ O ₃ -500	16.1	0.16	117.2	1.16	0.14
Ni/ γ -Al ₂ O ₃ -650	18.2	0.19	114.7	1.25	0.15
Ni/ γ -Al ₂ O ₃ -950	28.6	0.42	79.1	1.17	0.36
Ni/ γ -AlOOH-500	23.1	0.19	93.6	0.75	0.28
Ni/ γ -AlOOH-650	24.8	0.23	113.4	1.13	0.21
Ni/ γ -AlOOH-950	23.7	0.28	65.4	0.82	0.37
Ni/ α -Al ₂ O ₃	1.70	0.28	0.21	0.04	7.0

In addition, they showed tailing that extended over a wide range of elevated temperatures indicating the presence of strong acidic sites, which are typically Lewis acid sites, with considerable heterogeneity in their strength and density distribution. The Ni catalysts showed, generally, higher acid site density compared to γ -Al₂O₃, which would be expected as the Ni atoms in the dispersed Ni particles act as Lewis acid sites. The Ni/ α -Al₂O₃ catalyst showed negligible adsorption of NH₃, which can be referred to the crystalline corundum structure of the support where all Al³⁺ ions are octahedrally coordinated showing negligible Lewis acidity. In addition, the low surface areas of the support and the active metal minimize their contribution to the surface acid- base characteristics. Comparison between the two types of support precursors shows that Ni/ γ -AlOOH-500 possessed lower acidic site density compared to Ni/ γ -Al₂O₃-500, which correlates with the trend in their basic site density, that was explained based on the different structures of the support precursors. However, Ni/ γ -AlOOH-650 showed, relatively, high acidic site density comparable to Ni/ γ -Al₂O₃-650. These results indicate that Ni/ γ -AlOOH-650 possessed, relatively, high density of basic and acidic sites, which may reflect a significant contribution of acid-base pair

sites. This behavior may indicate that its moderate calcination temperature allowed for partial dehydroxylation, retaining some basic as well as acidic OH groups on the surface, besides exposing coordinatively unsaturated Al^{3+} Lewis acid and O^{2-} basic sites.

4.6 In-situ DRIFTS of Chemisorbed CO

Infrared spectra of CO molecules adsorbed on metal catalysts are very sensitive to the metal oxidation state and the coordination of the adsorbing metal atoms. Therefore, adsorption of CO was studied in-situ at room temperature, and the spectra of adsorbed molecules on $\text{Ni}/\gamma\text{-AlOOH-650}$ and $\text{Ni}/\alpha\text{-Al}_2\text{O}_3$ are shown in Figure 21.

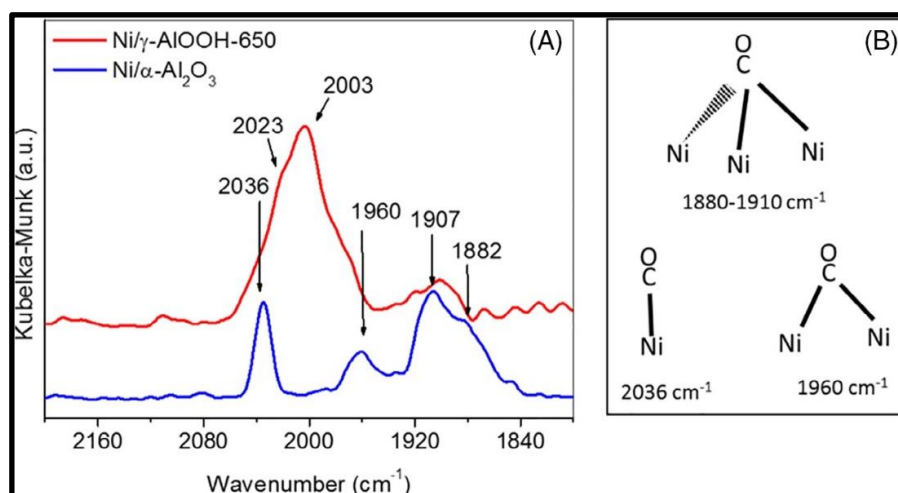


Figure 21: (DRIFTS) spectra of adsorbed CO on selected reduced catalysts. (A) and a schematic representation of CO adsorption modes (B).

The spectrum of adsorbed molecules on $\text{Ni}/\alpha\text{-Al}_2\text{O}_3$ showed peaks in three main spectral regions that correspond to different modes of CO binding to Ni^0 atoms. The peak at 2036 cm^{-1} is attributed to linearly adsorbed CO molecules, which usually indicate moderately dispersed Ni particles [68, 69]. The peaks below 2000 cm^{-1} indicate further weakening of the C-O bond due to stronger back-bonding, which

results in an enhanced electron density expansion from metal d-orbitals to the lowest unoccupied antibonding molecular orbital of CO. Therefore, the peaks at 1960, 1907, and 1882 cm^{-1} reflect different modes of CO molecules bound to more than one Ni atom at the same time in a bridging mode as shown in Figure 21B. Based on this, the peak at 1960 cm^{-1} can be assigned to CO molecules bridging two atoms, and the lower peaks can be referred to molecules bridging three nickel atoms. The presence of bridging CO molecules is often linked to poorly dispersed Ni particles [69] which agrees with the relatively low Ni dispersion in Ni/ α -Al₂O₃ measured by CO chemisorption, Table 3. The absence of peaks in the spectral region $>2100 \text{ cm}^{-1}$ is an evidence of the absence of adsorption on oxidized Ni sites (Niⁿ⁺) indicating that Ni exists only in the metallic (Ni⁰) state. These results agree with the XRD pattern of reduced Ni/ α -Al₂O₃ which showed only metallic Ni as the sole Ni species. They also correlate with the H₂-TPR results which showed high reducibility at relatively low temperatures. Interestingly, the spectrum of adsorbed CO on Ni/ γ -AlOOH-650 showed significantly different adsorption behavior compared to Ni/ α -Al₂O₃. Its spectrum is also different from the spectra usually observed for adsorption on γ -Al₂O₃-supported catalysts, which are usually close to the spectrum observed for Ni/ α -Al₂O₃ [69, 70]. It showed different overlapping peaks in the spectral region where linearly bonded CO molecules are expected, 2000 to 2040 cm^{-1} , indicating binding of CO molecules to Ni⁰ atoms with different degrees of strength, which also indicates binding to atoms of different coordination numbers. The fact that the highest intensity of the peak is centered in the lower frequency region, at 2003 cm^{-1} , indicates the dominance of Ni species with stronger interaction with the support surface and hence, stronger back-bonding to the CO molecules leading to weaker C-O bonds. The relatively weaker peaks $<2000 \text{ cm}^{-1}$ indicate the presence of less bridging CO molecules. It has been

reported, as a general trend, that an increase in the linearly adsorbed molecules indicates the dominance of small and dispersed metal particles [70]. These suggestions are well supported by the higher dispersion and the significantly smaller particle size obtained for this catalyst from the CO chemisorption study. The very weak peak observed in the spectral region $>2100\text{ cm}^{-1}$ indicates negligible adsorption on some $\text{Ni}^{\text{n+}}$ sites, confirming that zero-valent metal is the dominant Ni state. These results also agree with the H_2 -TPR results presented in Figure 17, where Ni/ γ -AlOOH-650 showed high reducibility with a profile expanding over a wide temperature range indicating different degrees of Ni-support interactions.

4.7 Catalytic Activity Tests

In reference experiments, where the reactor was not charged with a catalyst, a reaction was conducted under the same conditions applied in all catalytic activity tests, 700°C and 1 atm pressure. In these blank experiments, around 4% CH_4 conversion was observed where the products were mainly CO_2 and H_2O in addition to negligible amounts of H_2 and CO . The results of the catalytic activity tests over Ni/ γ - Al_2O_3 -derived catalysts are presented in Figure 22, where they are also compared with Ni/ α - Al_2O_3 . Ni/ α - Al_2O_3 showed considerably lower catalytic activity than all other catalysts, which can be explained by its highly crystalline support with its very low surface area, leading to lower metal surface area and larger crystals of Ni on the surface, as was confirmed by the CO chemisorption results. Besides lower conversion, Ni/ α - Al_2O_3 showed lower H_2 and higher CO_2 selectivity at cost of CO , leading to a H_2/CO ratio of around 2.2. In addition, the amount of water that was formed in the reaction over Ni/ α - Al_2O_3 was noticeably larger than that from reactions over all other catalysts. However, the TGA results of the spent catalysts showed that reactions over

Ni/ α -Al₂O₃ were associated with negligible amounts of coke deposits compared with most of the other catalysts, as shown in Table 6. The enhanced formation of CO₂ and H₂O over H₂, CO, and C may suggest that complete methane combustion (Reaction 9 below) takes place more favorably on the surface of Ni/ α -Al₂O₃ at cost of steam and CO₂ reforming (Reactions 9 and 11), which are believed to be the two main reaction steps leading to syngas.

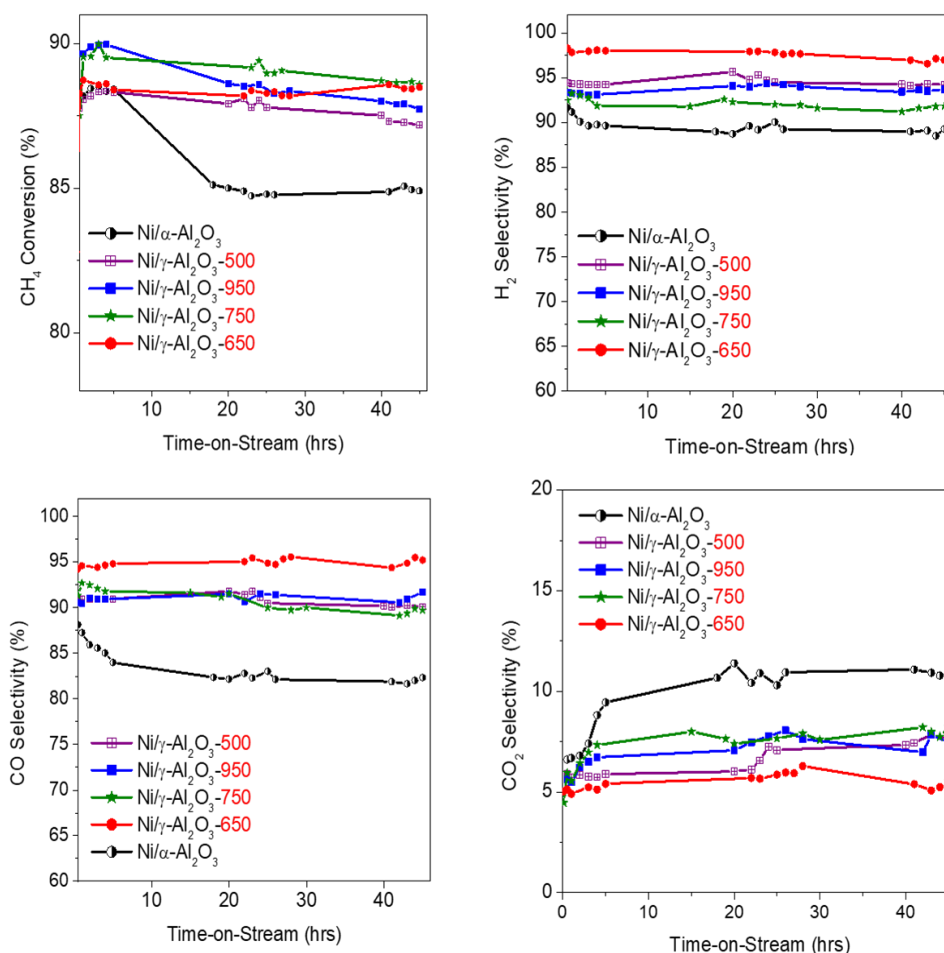
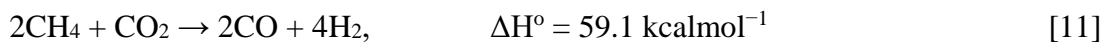
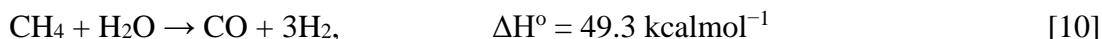
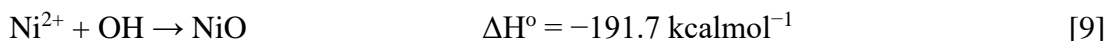


Figure 22: Catalytic activity of Ni/ γ -Al₂O₃-derived catalysts at 700°C, 1 atm, and 7605 mL CH₄ g⁻¹ h⁻¹. Each measurement is an average of the results of three or four experiments with reproducibility around 98%.

Reactions 9 to 11 are among a complex set of reactions that are believed to take place during catalytic POM over metal catalysts [71].



Compared to Ni/ α -Al₂O₃, all Ni/ γ -Al₂O₃-derived catalysts showed higher CH₄ conversion and higher selectivity to H₂ and CO. They all showed comparable conversions between 87% and 88% at the end of 45 hours on-stream. A negligible decrease (~1%) in the conversion was generally observed for most of them, which can be referred, in part, to the small amounts of coke deposits on their surfaces over time. Ni/ γ -Al₂O₃-650 showed a stable conversion associated with noticeably higher selectivity to H₂ and CO. This behavior could be explained by the higher thermal stability of its support compared to its counterpart, pretreated at 500°C, and compared to the others treated at higher temperatures where θ -Al₂O₃ started to form according to their XRD patterns.

Ni/ γ -AlOOH-derived catalysts, on the other hand, showed more noticeable dependence on the calcination temperature, as shown in Figure 23. Figure 24 also shows the average values of methane conversion, products' selectivity, and H₂/CO ratio over the 45 hours on-stream. While the catalysts calcined at 650°C and 750°C showed stable conversions, 87% to 88%, the catalysts calcined at 500°C and 950°C showed a noticeable decline in the conversion from 88.5% to around 86.5% and from 88% to 85%, respectively. Although all catalysts showed relatively small amounts of coke after reactions, Ni/ γ -AlOOH-500 showed more coke deposits compared to the other catalysts, Table 6, which could be the main reason behind its rapid deactivation. Coke formation and the type of carbon formed were also confirmed by Raman spectroscopy as shown in Figure 25. However, the catalyst calcined at 950°C showed

negligible amounts of carbon deposit, which indicates that its deactivation is related to a different factor, other than coking. Its deactivation is more likely due to the formation of NiAl_2O_4 as the sole Ni species, which is not as reducible as NiO under the employed reaction conditions.

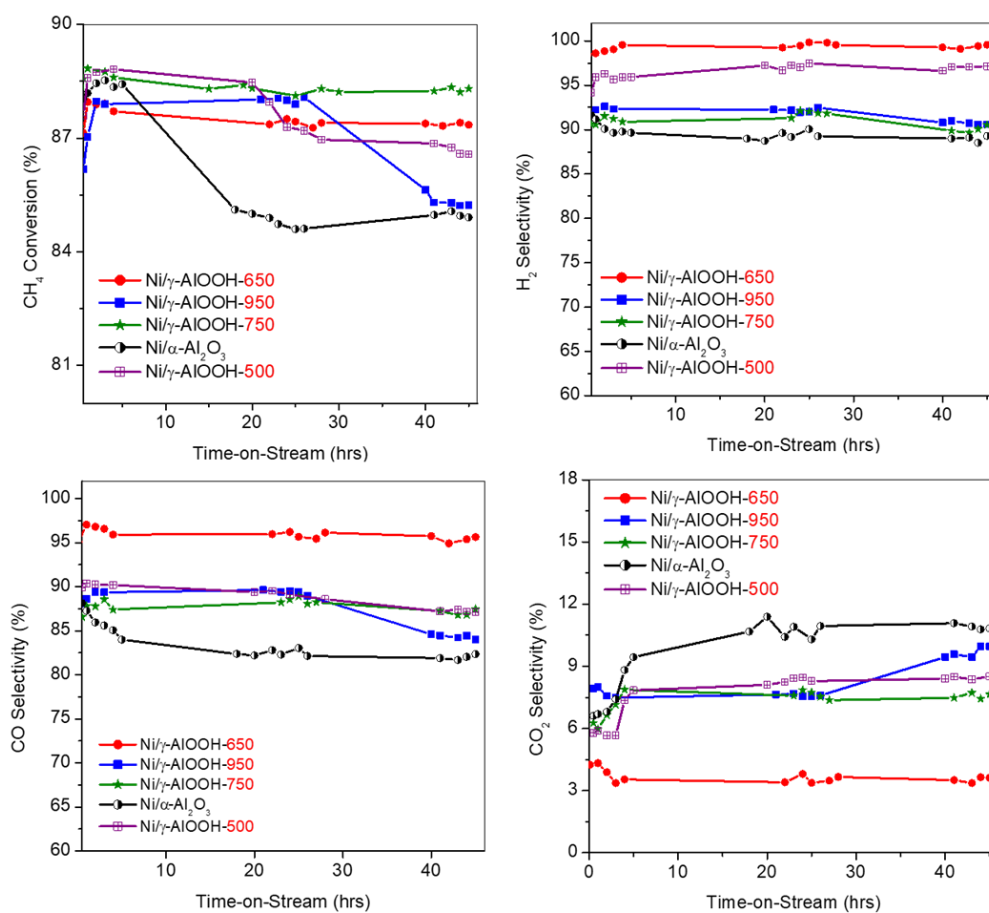


Figure 23: Catalytic activity of Ni/ γ -AlOOH-derived catalysts at 700°C, 1 atm, and 7605 mL CH₄ g⁻¹ h⁻¹.

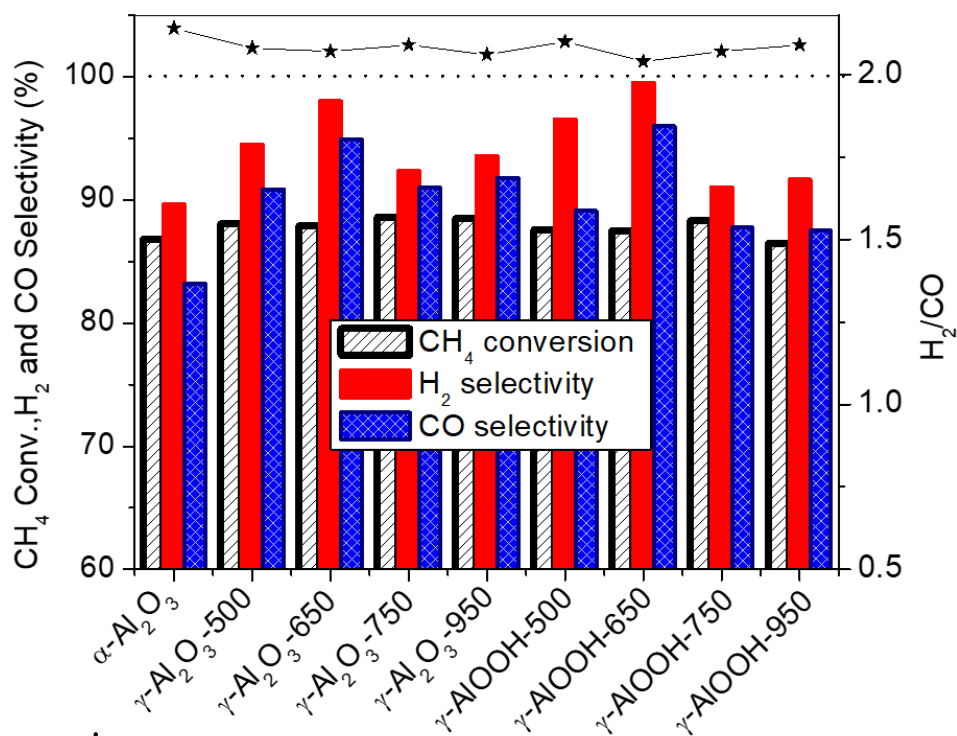


Figure 24: Averages of CH₄ conversion, products' selectivity, and H₂/CO ratio from 45-hour reactions over different catalysts at 700°C, 1 atm, and 7605 mL CH₄ g⁻¹ h⁻¹.

Interestingly, the Ni/ γ -AlOOH-650 catalyst, besides its stable promising conversion, showed noticeably higher selectivity to H₂ and CO compared to all other catalysts including the Ni/ γ -Al₂O₃ catalysts presented in Figure 22. The higher selectivity to syngas was on the account of CO₂ formation giving an average H₂/CO ratio of 2.04, which is very close to the value desired for the Fischer-Tropsch synthesis, 2.0. The stable conversion and the higher selectivity to syngas over Ni/ γ -AlOOH-650 may be explained, in part, due to its calcination temperature which is around the highest temperature at which a significant fraction of NiO can be retained before reaction with the support forming NiAl₂O₄, as was evident in its XRD pattern and was supported by H₂-TPR results. In addition, based on the CO chemisorption results, this catalyst showed noticeably higher Ni dispersion, larger metal surface area, and

smaller average Ni crystallites compared to the other catalysts. Furthermore, this catalyst exhibited, relatively, a high density of acid-base pairs as was confirmed by the TPD results. The unique textural and acid- base properties can be explained by the different structural characteristics of its support precursor, as described above in the discussion on CO chemisorption results. It is evident that these textural, structural, and chemical characteristics of the catalyst govern its catalytic performance and suppress the negative impact of the carbon deposits.

Table 6 also shows that the coke formation generally decreased as the calcination temperature increased, indicating a correlation between the amount of coke deposited and the structural stability of the support as well as the structure of active Ni phase. The results demonstrate that the catalysts based on θ - Al_2O_3 , at 950°C , and on the more structurally stable α - Al_2O_3 resulted in less coke formation compared to the catalysts where the support was γ - Al_2O_3 , especially with catalysts treated at 500°C and 650°C . The same trend was also observed for the γ - AlOOH -derived catalysts, which showed the highest amount of coke deposit over Ni/γ - AlOOH -500 and the lowest amount over Ni/γ - AlOOH -950, where NiAl_2O_4 was observed as the sole Ni species. In each set of catalysts, the amount of carbon deposit seems to correlate with the acid/base density ratio presented in Table 5, where the carbon deposit decreased as the ratio increased, which agrees with similar studies that reported suppression of carbon deposits by increasing the basicity of the catalysts [72, 73]. However, as discussed above, other factors including textural, structural, and acid-base characteristics seemed to play a key role in the catalytic activity minimizing the effect of the carbon deposits. Raman spectra of the spent catalysts were recorded for further characterization of the coke deposits as shown in Figure 25.

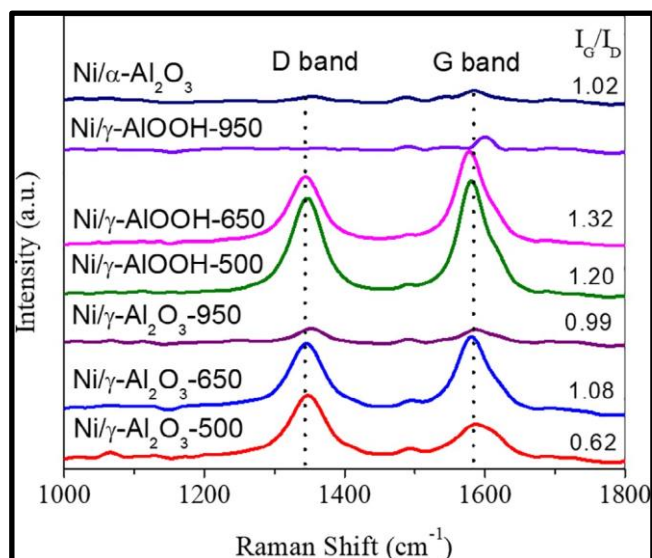


Figure 25: Carbon deposit on spent catalysts

Table 6: Carbon deposit on spent catalysts

Catalyst	Amount of carbon ($\text{g}_\text{C} \text{g}^{-1} \text{catal.}$)	Average coking rate ($\text{g}_\text{C} \text{g}^{-1} \text{catal} \text{h}^{-1}$)
Ni/ α - Al_2O_3	0.03	0.0007
Ni/ γ - Al_2O_3 -500	0.07	0.0016
Ni/ γ - Al_2O_3 -650	0.06	0.0013
Ni/ γ - Al_2O_3 -750	0.035	0.0008
Ni/ γ - Al_2O_3 -950	0.027	0.0006
Ni/ γ - Al_2O_3 -1100	0.027	0.0006
Ni/ γ -AlOOH-500	0.12	0.003
Ni/ γ -AlOOH-650	0.09	0.002
Ni/ γ -AlOOH-750	0.06	0.0013
Ni/ γ -AlOOH-950	0.03	0.0007

All catalysts showed two characteristic carbon bands centering at 1345 and 1580 cm^{-1} . The intensity of the peaks in the spectra correlate with the TGA results presented in Table 5. The two bands are usually assigned to D (1345 cm^{-1}) and G (1580 cm^{-1}) vibration modes of carbonaceous species [74, 75]. The D band is usually assigned to disordered carbon filaments, carbon nanoparticles, or amorphous carbon, while the G

band is assigned to the sp^2 C-C vibrations of ordered graphitic carbon. It was also noticed that the weak G band of Ni/ γ -AlOOH-950, where NiAl₂O₄ was the sole Ni species before reduction, appeared at a higher wavenumber value of 1600 cm^{-1} . This shift in the band could be due to some unusual structural disorder as was suggested in similar literature reports where a peak around 1610 cm^{-1} was assigned to disordered aromatic structures [74]. It has been accepted that the graphitized carbon has a higher negative impact on the catalytic activity, which correlate with its lower tendency to be gasified compared with disordered carbon and carbon nanostructures. All tested catalysts presented in Figure 25 showed both types of carbon with small variation in the G/D band intensity ratio, IG/ID. The Ni/ γ -AlOOH catalysts showed relatively higher IG/ID ratios compared to their Ni/ γ -Al₂O₃ counter- parts. The same catalysts also showed higher base/acid site density ratios, Table 5, but further studies would be needed to prove any relationship between the two characteristics and their effect on the catalytic performance. In view of these results, it is evident that the structural, the textural, and the surface properties of the starting support, play a key role in the textural and morphological characteristics of the metal active phase, and in its catalytic performance as well as in the mechanisms of the reactions involved. The reported results herein provide a strong evidence that impregnation of γ -AlOOH, as an alternative to γ -Al₂O₃ and α -Al₂O₃, followed by moderate calcination, can be a promising alternative route to produce efficient catalysts with enhanced dispersion of Ni nanoparticles and enhanced syngas selectivity in POM, with a H₂/CO ratio very close to 2.0. While the results also give some insight into correlations between Ni textural properties and the mechanisms involved, more work is still undergoing for better understanding of such correlations, including kinetic studies and in situ Fourier-transform infrared (FTIR) study of CH₄ adsorption. Undergoing work also involves

studies on modifying the Ni/ γ -AlOOH-derived catalysts, by doping with other elements, in efforts to further minimize coke formation.

Chapter 5: Conclusion

Promising Ni nano catalysts were prepared through a new route employing γ -AlOOH as a support precursor followed by calcination at different temperatures. The textural properties of the γ -AlOOH-derived catalysts and their catalytic performance in POM were compared with corresponding catalysts prepared over γ -Al₂O₃, and α -Al₂O₃. The structural, textural, and surface properties of the support precursor showed a strong influence on the type of Ni active phase and its interaction with the support, which eventually played a key role in the catalytic performance. When γ -AlOOH was impregnated with the Ni precursor, NiO was the dominant Ni species after calcination at moderate temperatures, 500°C to 650°C, which reacted with the support at higher temperatures forming NiAl₂O₄ as the sole Ni species. On the other hand, when γ -Al₂O₃ support was calcined at different temperatures (500-1100°C) before impregnation, mixtures of NiO and NiAl₂O₄ were obtained regardless of the calcination temperature of the support. Furthermore, γ -AlOOH-derived catalysts showed higher specific surface areas and mesopores of smaller average diameter.

The structural and the surface properties of the starting support play a key role in the textural and morphological characteristics of the Ni active species. γ -AlOOH-derived catalysts exhibited higher Ni dispersion, larger metal surface area and smaller Ni crystallites than all other catalysts, which was explained based on the surface properties of the support, γ -AlOOH. The modified textural characteristics of the Ni particles in these catalysts, combined with calcination at a moderate temperature, 650°C, resulted in an improved performance in POM, including stable CH₄ conversion and enhanced selectivity to syngas with a H₂/CO ratio very close to 2.0. The results of this study show that more efficient Ni nano catalysts can be prepared by impregnation

of γ -AlOOH as a promising alternative support precursor followed by careful calcination at moderate temperatures.

References

1. Velasco, C. Fernandez, L. Lopez, S. Cabrera, M. Boutonnet and S. Järås, "Catalytic partial oxidation of methane over nickel and ruthenium-based catalysts under low O₂/CH₄ ratios and with addition of steam", *Fuel*, vol. 153, pp. 192-201, 2015.
2. Christian Enger, R. Lødeng and A. Holmen, "A review of catalytic partial oxidation of methane to synthesis gas with emphasis on reaction mechanisms over transition metal catalysts", *Applied Catalysis A: General*, vol. 346, no. 1-2, pp. 1-27, 2008.
3. A. York, "Brief Overview of the Partial Oxidation of Methane to Synthesis Gas", *Topics in Catalysis*, vol. 22, no. 34, pp. 345-358, 2003.
4. A. Bodke, D. Olschki and L. Schmidt, "Hydrogen addition to the Andrussov process for HCN synthesis", *Applied Catalysis A: General*, vol. 201, no. 1, pp. 13-22, 2000.
5. M. Diefenbach, M. Brönstrup, M. Aschi, D. Schröder and H. Schwarz, "HCN Synthesis from Methane and Ammonia: Mechanisms of Pt⁺-Mediated C–N Coupling", *Journal of the American Chemical Society*, vol. 121, no. 45, pp. 10614-10625, 1999.
6. H. Gesser, N. Hunter and C. Prakash, "The direct conversion of methane to methanol by controlled oxidation", *Chemical Reviews*, vol. 85, no. 4, pp. 235-244, 1985.
7. T. Yabe, Y. Kamite, K. Sugiura, S. Ogo and Y. Sekine, "Low-temperature oxidative coupling of methane in an electric field using carbon dioxide over Ca-doped LaAlO₃ perovskite oxide catalysts", *Journal of CO₂ Utilization*, vol. 20, pp. 156-162, 2017.
8. A. Behroozsarand and A. Zamaniyan, "Simulation and optimization of an integrated GTL process", *Journal of Cleaner Production*, vol. 142, pp. 2315-2327, 2017.
9. M. Bassiony, A. Ibrahim and M. El-Kassaby, "An experimental study on the effect of using gas-to-liquid (GTL) fuel on diesel engine performance and emissions", *Alexandria Engineering Journal*, vol. 55, no. 3, pp. 2115-2124, 2016.

10. G. Santos, O. Basha, R. Wang, H. Ashkanani and B. Morsi, "Techno-economic assessment of Fischer-Tropsch synthesis and direct methane-to-methanol processes in modular GTL reactors", *Catalysis Today*, vol. 371, pp. 93-112, 2021.
11. T. Choudhary and V. Choudhary, "Energy-Efficient Syngas Production through Catalytic Oxy-Methane Reforming Reactions", *Angewandte Chemie International Edition*, vol. 47, no. 10, pp. 1828-1847, 2008.
12. A. Stranges, "A History of the Fischer-Tropsch Synthesis in Germany 1926–45", *Studies in Surface Science and Catalysis*, pp. 1-27, 2007.
13. V. Dieterich, A. Buttler, A. Hanel, H. Spliethoff and S. Fendt, "Power-to-liquid via synthesis of methanol, DME or Fischer–Tropsch-fuels: a review", *Energy & Environmental Science*, vol. 13, no. 10, pp. 3207-3252, 2020.
14. N. Nielsen, A. Jensen and J. Christensen, "The roles of CO and CO₂ in high pressure methanol synthesis over Cu-based catalysts", *Journal of Catalysis*, vol. 393, pp. 324-334, 2021.
15. A. Klerk, "Engineering evaluation of direct methane to methanol conversion", *Energy Science & Engineering*, vol. 3, no. 1, pp. 60-70, 2014.
16. L. Milner-Elkharouf, M. Khzouz and R. Steinberger-Wilckens, "Catalyst development for indirect internal reforming (IIR) of methane by partial oxidation", *International Journal of Hydrogen Energy*, vol. 45, no. 8, pp. 5285-5296, 2020.
17. P. Li, X. Chen, Y. Li and J. Schwank, "A review on oxygen storage capacity of CeO₂-based materials: Influence factors, measurement techniques, and applications in reactions related to catalytic automotive emissions control", *Catalysis Today*, vol. 327, pp. 90-115, 2019.
18. Villa, P., and Nardini, A., "Catalytic industrial processes carried out at high temperature on precious metals", *International Review of Chemical Engineering*, vol. 3. no. 5, pp. 515-529, 2011.
19. S. Al-Sayari, "Recent Developments in the Partial Oxidation of Methane to Syngas", *The Open Catalysis Journal*, vol. 6, no. 1, pp. 17-28, 2013.
20. P. Munnik, P. de Jongh and K. de Jong, "Recent Developments in the Synthesis of Supported Catalysts", *Chemical Reviews*, vol. 115, no. 14, pp. 6687-6718, 2015.

21. Y. XU et al., "A comparison of Al₂O₃ and SiO₂ supported Ni-based catalysts in their performance for the dry reforming of methane", *Journal of Fuel Chemistry and Technology*, vol. 47, no. 2, pp. 199-208, 2019.
22. R. Kumar Singha et al., "Synthesis effects on activity and stability of Pt-CeO₂ catalysts for partial oxidation of methane", *Molecular Catalysis*, vol. 432, pp. 131-143, 2017.
23. S. Vives, C. Guizard, L. Cot and C. Oberlin, "Sol-gel/co-precipitation method for the preparation and characterization of zirconia-tungsten composite powders", *Journal of Materials Science*, vol. 34, no. 13, pp. 3127-3135, 1999.
24. A. Giuliano, C. Freda and E. Catizzone, "Techno-Economic Assessment of Bio-Syngas Production for Methanol Synthesis: A Focus on the Water-Gas Shift and Carbon Capture Sections", *Bioengineering*, vol. 7, no. 3, p. 70, 2020.
25. K. Xiao, Q. Wang, X. Qi and L. Zhong, "For Better Industrial Cu/ZnO/Al₂O₃ Methanol Synthesis Catalyst: A Compositional Study", *Catalysis Letters*, vol. 147, no. 6, pp. 1581-1591, 2017.
26. H. Figen and S. Baykara, "Hydrogen production by partial oxidation of methane over Co based, Ni and Ru monolithic catalysts", *International Journal of Hydrogen Energy*, vol. 40, no. 24, pp. 7439-7451, 2015.
27. C. Ding et al., "One step synthesis of mesoporous NiO-Al₂O₃ catalyst for partial oxidation of methane to syngas: The role of calcination temperature", *Fuel*, vol. 162, pp. 148-154, 2015.
28. S. Sharifian and N. Asasian-Kolur, "Studies on CO_x hydrogenation to methane over Rh-based catalysts", *Inorganic Chemistry Communications*, vol. 118, p. 108021, 2020.
29. D. Costa et al., "Study of nickel, lanthanum and niobium-based catalysts applied in the partial oxidation of methane", *Catalysis Today*, vol. 344, pp. 15-23, 2020.
30. D. Kaddeche, A. Djaidja and A. Barama, "Partial oxidation of methane on co-precipitated Ni-Mg/Al catalysts modified with copper or iron", *International Journal of Hydrogen Energy*, vol. 42, no. 22, pp. 15002-15009, 2017.
31. J. Zhou, H. Ma, F. Jin, H. Zhang and W. Ying, "Mn and Mg dual promoters modified Ni/ α -Al₂O₃ catalysts for high temperature syngas methanation", *Fuel Processing Technology*, vol. 172, pp. 225-232, 2018.

32. G. Figueredo et al., "A comparative study of dry reforming of methane over nickel catalysts supported on perovskite-type LaAlO_3 and commercial $\alpha\text{-Al}_2\text{O}_3$ ", *International Journal of Hydrogen Energy*, vol. 43, no. 24, pp. 11022-11037, 2018.
33. S. Hassani Rad, M. Haghghi, A. Alizadeh Eslami, F. Rahmani and N. Rahemi, "Sol-gel vs. impregnation preparation of MgO and CeO_2 doped $\text{Ni/Al}_2\text{O}_3$ nanocatalysts used in dry reforming of methane: Effect of process conditions, synthesis method and support composition", *International Journal of Hydrogen Energy*, vol. 41, no. 11, pp. 5335-5350, 2016.
34. H. Özdemir and M. Faruk Öksüzömer, "Synthesis of Al_2O_3 , MgO and MgAl_2O_4 by solution combustion method and investigation of performances in partial oxidation of methane", *Powder Technology*, vol. 359, pp. 107-117, 2020.
35. R. Singha, A. Shukla, A. Yadav, L. Sivakumar Konathala and R. Bal, "Effect of metal-support interaction on activity and stability of Ni-CeO_2 catalyst for partial oxidation of methane", *Applied Catalysis B: Environmental*, vol. 202, pp. 473-488, 2017.
36. K. Roseno, R. Brackmann, M. da Silva and M. Schmal, "Investigation of LaCoO_3 , LaFeO_3 and $\text{LaCo}_{0.5}\text{Fe}_{0.5}\text{O}_3$ perovskites as catalyst precursors for syngas production by partial oxidation of methane", *International Journal of Hydrogen Energy*, vol. 41, no. 40, pp. 18178-18192, 2016.
37. C. Silva, L. da Conceição, N. Ribeiro and M. Souza, "Partial oxidation of methane over Ni-Co perovskite catalysts", *Catalysis Communications*, vol. 12, no. 7, pp. 665-668, 2011.
38. A. Ferreira et al., "Partial oxidation of methane over bimetallic copper- and nickel-actinide oxides (Th, U)", *Journal of Alloys and Compounds*, vol. 497, no. 1-2, pp. 249-258, 2010.
39. L. Mattos, "Partial oxidation of methane on Pt/Ce-ZrO_2 catalysts", *Catalysis Today*, vol. 77, no. 3, pp. 245-256, 2002.
40. C. Alvarez-Galvan et al., "Partial Oxidation of Methane to Syngas Over Nickel-Based Catalysts: Influence of Support Type, Addition of Rhodium, and Preparation Method", *Frontiers in Chemistry*, vol. 7, 2019. doi: 10.3389/fchem.2019.00104

41. W. Duan, R. Wentzcovitch and K. Thomson, "First-principles study of high-pressure alumina polymorphs", *Physical Review B*, vol. 57, no. 17, pp. 10363-10369, 1998.
42. E. Rytter, Ø. Borg, B. Enger and A. Holmen, " α -alumina as catalyst support in Co Fischer-Tropsch synthesis and the effect of added water; encompassing transient effects", *Journal of Catalysis*, vol. 373, pp. 13-24, 2019.
43. M. Yamasaki, H. Habazaki, K. Asami, K. Izumiya and K. Hashimoto, "Effect of tetragonal ZrO₂ on the catalytic activity of Ni/ZrO₂ catalyst prepared from amorphous Ni-Zr alloys", *Catalysis Communications*, vol. 7, no. 1, pp. 24-28, 2006.
44. S. Wang, H. Niu, M. Guo, J. Wang, T. Chen and G. Wang, "Effect of zirconia polymorph on the synthesis of diphenyl carbonate over supported lead catalysts", *Molecular Catalysis*, vol. 468, pp. 117-124, 2019.
45. W. Liu, L. Li, X. Zhang, Z. Wang, X. Wang and H. Peng, "Design of Ni-ZrO₂@SiO₂ catalyst with ultra-high sintering and coking resistance for dry reforming of methane to prepare syngas", *Journal of CO₂ Utilization*, vol. 27, pp. 297-307, 2018.
46. M. Cai, J. Wen, W. Chu, X. Cheng and Z. Li, "Methanation of carbon dioxide on Ni/ZrO₂-Al₂O₃ catalysts: Effects of ZrO₂ promoter and preparation method of novel ZrO₂-Al₂O₃ carrier", *Journal of Natural Gas Chemistry*, vol. 20, no. 3, pp. 318-324, 2011.
47. Q. ZHANG, M. SHEN, J. WEN, J. WANG and Y. FEI, "Partial oxidation of methane on Ni/CeO₂-ZrO₂/ γ -Al₂O₃ prepared using different processes", *Journal of Rare Earths*, vol. 26, no. 3, pp. 347-351, 2008.
48. S. Ikram et al., "A novel approach to simultaneously enhance the Seebeck coefficient and electrical conductivity in rutile phase of TiO₂ nanostructures", *Arabian Journal of Chemistry*, vol. 13, no. 8, pp. 6724-6729, 2020.
49. M. Shah, A. Bordoloi, A. Nayak and P. Mondal, "Effect of Ti/Al ratio on the performance of Ni/TiO₂-Al₂O₃ catalyst for methane reforming with CO₂", *Fuel Processing Technology*, vol. 192, pp. 21-35, 2019.

50. M. LAZARO, Y. ECHEGOYEN, C. ALEGRE, I. SUELVES, R. MOLINER and J. PALACIOS, "TiO₂ as textural promoter on high loaded Ni catalysts for methane decomposition", *International Journal of Hydrogen Energy*, vol. 33, no. 13, pp. 3320-3329, 2008.
51. X. Lin, L. Lin, K. Huang, X. Chen, W. Dai and X. Fu, "CO methanation promoted by UV irradiation over Ni/TiO₂", *Applied Catalysis B: Environmental*, vol. 168-169, pp. 416-422, 2015.
52. T. Hansen, A. DeLaRiva, S. Challa and A. Datye, "Sintering of Catalytic Nanoparticles: Particle Migration or Ostwald Ripening?", *Accounts of Chemical Research*, vol. 46, no. 8, pp. 1720-1730, 2013.
53. X. Bai, S. Wang, T. Sun and S. Wang, "The sintering of Ni/Al₂O₃ methanation catalyst for substitute natural gas production", *Reaction Kinetics, Mechanisms and Catalysis*, vol. 112, no. 2, pp. 437-451, 2014.
54. P. Voorhees, "The theory of Ostwald ripening", *Journal of Statistical Physics*, vol. 38, no. 1-2, pp. 231-252, 1985.
55. S. Challa et al., "Relating Rates of Catalyst Sintering to the Disappearance of Individual Nanoparticles during Ostwald Ripening", *Journal of the American Chemical Society*, vol. 133, no. 51, pp. 20672-20675, 2011.
56. R. van den Berg et al., "Support Functionalization to Retard Ostwald Ripening in Copper Methanol Synthesis Catalysts", *ACS Catalysis*, vol. 5, no. 7, pp. 4439-4448, 2015.
57. I. Yentekakis et al., "Stabilization of catalyst particles against sintering on oxide supports with high oxygen ion lability exemplified by Ir-catalyzed decomposition of N₂O", *Applied Catalysis B: Environmental*, vol. 192, pp. 357-364, 2016.
58. S. Singh, V. Srivastava, T. Mandal and I. Mall, "Synthesis of different crystallographic Al₂O₃ nanomaterials from solid waste for application in dye degradation", *RSC Adv.*, vol. 4, no. 92, pp. 50801-50810, 2014.
59. T. Tangcharoen, J. T-Thienprasert and C. Kongmark, "Effect of calcination temperature on structural and optical properties of MAl₂O₄ (M = Ni, Cu, Zn) aluminate spinel nanoparticles", *Journal of Advanced Ceramics*, vol. 8, no. 3, pp. 352-366, 2019.

60. Q. Liu, J. Sun, Q. Feng, S. Ji and Z. Wang, "A La-promoted Ni/MgAl₂O₄ catalyst with superior methanation performance for the production of synthetic natural gas", *Catalysis Today*, vol. 339, pp. 127-134, 2020.
61. M. Tan, X. Wang, X. Wang, X. Zou, W. Ding and X. Lu, "Influence of calcination temperature on textural and structural properties, reducibility, and catalytic behavior of mesoporous γ -alumina-supported Ni–Mg oxides by one-pot template-free route", *Journal of Catalysis*, vol. 329, pp. 151-166, 2015.
62. J. Zhang, H. Xu, X. Jin, Q. Ge and W. Li, "Characterizations and activities of the nano-sized Ni/Al₂O₃ and Ni/La–Al₂O₃ catalysts for NH₃ decomposition", *Applied Catalysis A: General*, vol. 290, no. 1-2, pp. 87-96, 2005.
63. R. López-Fonseca, C. Jiménez-González, B. de Rivas and J. Gutiérrez-Ortiz, "Partial oxidation of methane to syngas on bulk NiAl₂O₄ catalyst. Comparison with alumina supported nickel, platinum and rhodium catalysts", *Applied Catalysis A: General*, vol. 437-438, pp. 53-62, 2012.
64. L. Samain et al., "Structural analysis of highly porous γ -Al₂O₃", *Journal of Solid State Chemistry*, vol. 217, pp. 1-8, 2014.
65. E. Choi et al., "Cu/ZnO/AlOOH catalyst for methanol synthesis through CO₂ hydrogenation", *Korean Journal of Chemical Engineering*, vol. 35, no. 1, pp. 73-81, 2017.
66. L. Coleman, W. Epling, R. Hudgins and E. Croiset, "Ni/Mg–Al mixed oxide catalyst for the steam reforming of ethanol", *Applied Catalysis A: General*, vol. 363, no. 1-2, pp. 52-63, 2009.
67. F. Wang, W. Li, J. Lin, Z. Chen and Y. Wang, "Crucial support effect on the durability of Pt/MgAl₂O₄ for partial oxidation of methane to syngas", *Applied Catalysis B: Environmental*, vol. 231, pp. 292-298, 2018.
68. C. BARTHOLOMEW, "The stoichiometry of hydrogen and carbon monoxide chemisorption on alumina- and silica-supported nickel", *Journal of Catalysis*, vol. 65, no. 2, pp. 390-401, 1980.
69. F. Azzolina-Jury, "Novel boehmite transformation into γ -alumina and preparation of efficient nickel base alumina porous extrudates for plasma-assisted CO₂ methanation", *Journal of Industrial and Engineering Chemistry*, vol. 71, pp. 410-424, 2019.

70. X. Zhu, Y. Zhang and C. Liu, "CO Adsorbed Infrared Spectroscopy Study of Ni/Al₂O₃ Catalyst for CO₂ Reforming of Methane", *Catalysis Letters*, vol. 118, no. 3-4, pp. 306-312, 2007.
71. R. HORN et al., "Methane catalytic partial oxidation on autothermal Rh and Pt foam catalysts: Oxidation and reforming zones, transport effects, and approach to thermodynamic equilibrium", *Journal of Catalysis*, vol. 249, no. 2, pp. 380-393, 2007.
72. V. Thyssen, F. Georgetti and E. Assaf, "Influence of MgO content as an additive on the performance of Ni/MgO SiO₂ catalysts for the steam reforming of glycerol", *International Journal of Hydrogen Energy*, vol. 42, no. 27, pp. 16979-16990, 2017.
73. J. Du et al., "A strategy to regenerate coked and sintered Ni/Al₂O₃ catalyst for methanation reaction", *International Journal of Hydrogen Energy*, vol. 43, no. 45, pp. 20661-20670, 2018.
74. D. Xu, Y. Xiong, J. Ye, Y. Su, Q. Dong and S. Zhang, "Performances of syngas production and deposited coke regulation during co-gasification of biomass and plastic wastes over Ni/ γ -Al₂O₃ catalyst: Role of biomass to plastic ratio in feedstock", *Chemical Engineering Journal*, vol. 392, p. 123728, 2020.
75. Y. Li et al., "Coke formation on the surface of Ni/HZSM-5 and Ni-Cu/HZSM-5 catalysts during bio-oil hydrodeoxygenation", *Fuel*, vol. 189, pp. 23-31, 2017.

List of Publications

A. Khaleel, S. Jobe, M. Ahmed, S. Al-Zuhair and S. Tariq, "Enhanced selectivity of syngas in partial oxidation of methane: A new route for promising Ni-alumina catalysts derived from Ni/ γ -AlOOH with modified Ni dispersion", International Journal of Energy Research, vol. 44, no. 14, pp. 12081-12099, 2020. Available: [10.1002/er.5869](https://doi.org/10.1002/er.5869).